



# **APPENDIX 9**

## **BREATHE LONDON HOTSPOT ANALYSIS REPORT**

## D3.2 Hotspot Analysis

Final Report

*Breathe London Project*

*23 October 2020*

## Report Information

---

CERC Job Number: FM1196  
Job Title: D3.2 Hotspot Analysis  
Prepared for: EDF  
Report Status: Final  
Report Reference: FM1196/D3.2/R2/20  
Issue Date: 23 October 2020

---

Author(s): Amy Stidworthy, Ella Forsyth

---

Reviewer(s): David Carruthers

---

Issue	Date	Comments
1	27/07/20	Draft
2	23/10/20	Final

---

# Contents

<b>1. INTRODUCTION</b>	<b>4</b>
<b>2. METHODOLOGY</b>	<b>5</b>
2.1 ADMS-URBAN MODEL SETUP	5
2.1.1 Emissions	5
2.1.2 Meteorology	6
2.1.3 Background	6
2.2 MEASURED DATA	7
2.2.1 Static Measurement Sites	7
2.2.2 Mobile measurements	7
<b>3. RESULTS</b>	<b>8</b>
3.1 STATIC SITES	8
3.2 MOBILE LOCATIONS	21
3.2.1 NOX	23
3.2.2 NO2	24
3.2.3 PM10	25
3.2.4 PM2.5	26
3.2.5 Ozone	27
3.2.6 CO2	28
3.3 MOBILE LOCATIONS – CONTINUOUS MODELLING	29
<b>4. HOTSPOT ANALYSIS</b>	<b>35</b>
4.1 HANGAR LANE GYRATORY, EALING (EA6)	35
4.2 HOLLOWAY BUS GARAGE, ISLINGTON (54245)	37
4.3 LAMBETH – BRIXTON ROAD (LB4)	38
4.4 CROYDON – PURLEY WAY A23 (CR7)	39
4.5 CITY OF LONDON – BEECH STREET (CT4)	40
4.6 WESTMINSTER – STRAND (NORTHBANK BID) (NB1)	41
4.7 KINGSTON – LONDON ROAD (18245)	43
4.8 BARKING AND DAGENHAM – STATION PARADE (37245)	45
4.9 HACKNEY – CECILIA ROAD (78245)	47
4.10 HILLINGDON – RUISLIP HIGH STREET (92245)	49
4.11 SOUTHWARK – NEW KENT ROAD	51
4.12 EMBANKMENT	52
<b>5. DISCUSSION AND RECOMMENDATIONS</b>	<b>53</b>
5.1 LAEI ISSUES	53
5.2 TIME-VARYING EMISSIONS PROFILES	53
5.3 MONITOR LOCATION ADJUSTMENTS	53
5.4 QUEUING	53
5.5 REMAINING ISSUES	53
<b>APPENDIX A: SUMMARY OF ADMS-URBAN</b>	<b>54</b>

# 1. Introduction

Throughout the Breathe London project, CERC has compared measured concentrations with simulated concentrations from the ADMS-Urban air quality model. This process helps to identify potential refinements in the modelling approach, to identify issues with monitoring data and also to identify areas where the London Atmospheric Emissions Inventory (LAEI) used in the modelling could be improved. In this report, we have compared hourly modelled and measured concentrations at all Breathe London AQMesh, London Air Quality Network (LAQN) and Air Quality England (AQE) sites in Greater London for NO<sub>x</sub>, NO<sub>2</sub>, PM<sub>10</sub>, PM<sub>2.5</sub> and Ozone. We have also compared modelled and measured concentrations on all roads driven by the two Breathe London Google Cars during the project for NO<sub>x</sub>, NO<sub>2</sub>, PM<sub>10</sub>, PM<sub>2.5</sub>, Ozone and CO<sub>2</sub>, which gives a unique insight into areas not covered by static monitors. We have used qualitative and quantitative measures to assess overarching trends and have carried out a detailed analysis of a selection of “hotspots” where there is a notable model bias; in these locations high-resolution contour plots of concentrations and supporting information such as maps of traffic flows have been used to identify potential causes of differences. Section 2 describes the assessment methodology; Section 3 contains the overall results; Section 4 contains more detailed of analysis of the identified “hotspots” and Section 5 contains some recommendations for improvements. Appendix A contains detailed information about the ADMS-Urban model.

## 2. Methodology

### 2.1 ADMS-Urban model setup

#### 2.1.1 Emissions

The modelling used the London Atmospheric Emissions Inventory (LAEI) 2013 dataset, interpolated to 2019 emissions data for the modelled roads. The emissions contained “real world” adjustments<sup>1</sup> for NO<sub>2</sub> and NO<sub>x</sub>. The model also contained 35 point sources, major over ground rail links and aircraft sources to correctly account for the pollution due to Heathrow Airport and London’s biggest industrial sites and railways. The emissions for any other sources (domestic and commercial fuel combustion, minor roads, shipping etc.) that are not explicitly modelled were aggregated into 1km square grid cells. The grid cells are square volume sources with a depth of 10m that cover the region inside the M25, in accordance with the extent of the LAEI dataset.

##### 2.1.1.1 Time-varying emissions profiles

For this modelling exercise, new time-varying emissions profiles were developed to more accurately represent differences in vehicle types. Each modelled road was classified by location (Central, Inner, Outer and Motorway) and type (A Road Single or Dual Carriageway, B Road, Minor Road, Local Street, Motorway). Not all types are in every location, so there are 17 road categories. All roads in each category were grouped together, and average flows for each road category in terms of 11 vehicle categories were calculated. Then, DfT raw traffic flow data for London in 2018 were used to derive diurnal flow profiles for each vehicle category (DfT data only available weekdays between 07:00 and 18:00). These traffic flow diurnal profiles were then applied to the average emissions from each vehicle category, to develop pollutant-dependent emissions profiles for each of the 17 different road categories (Figure 2-1).

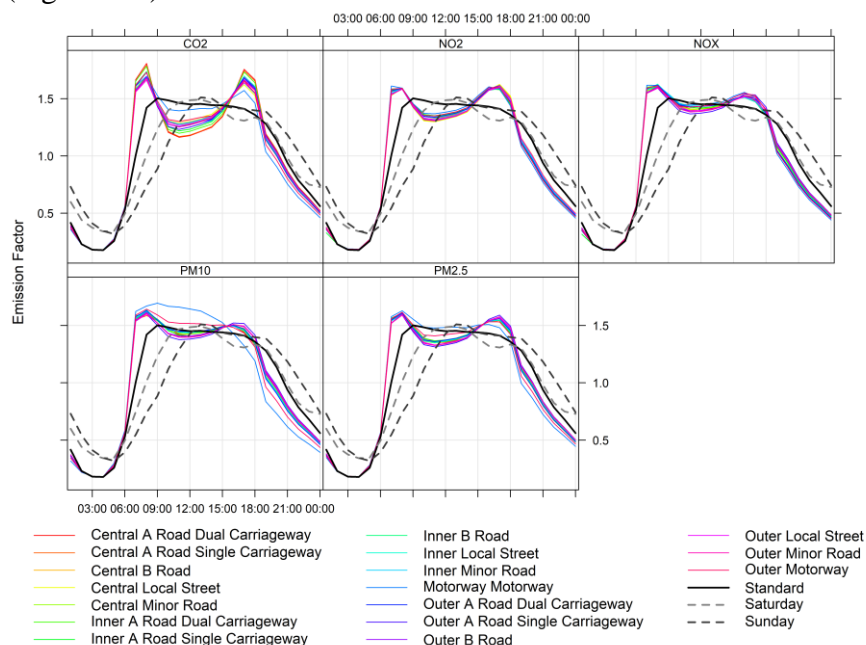
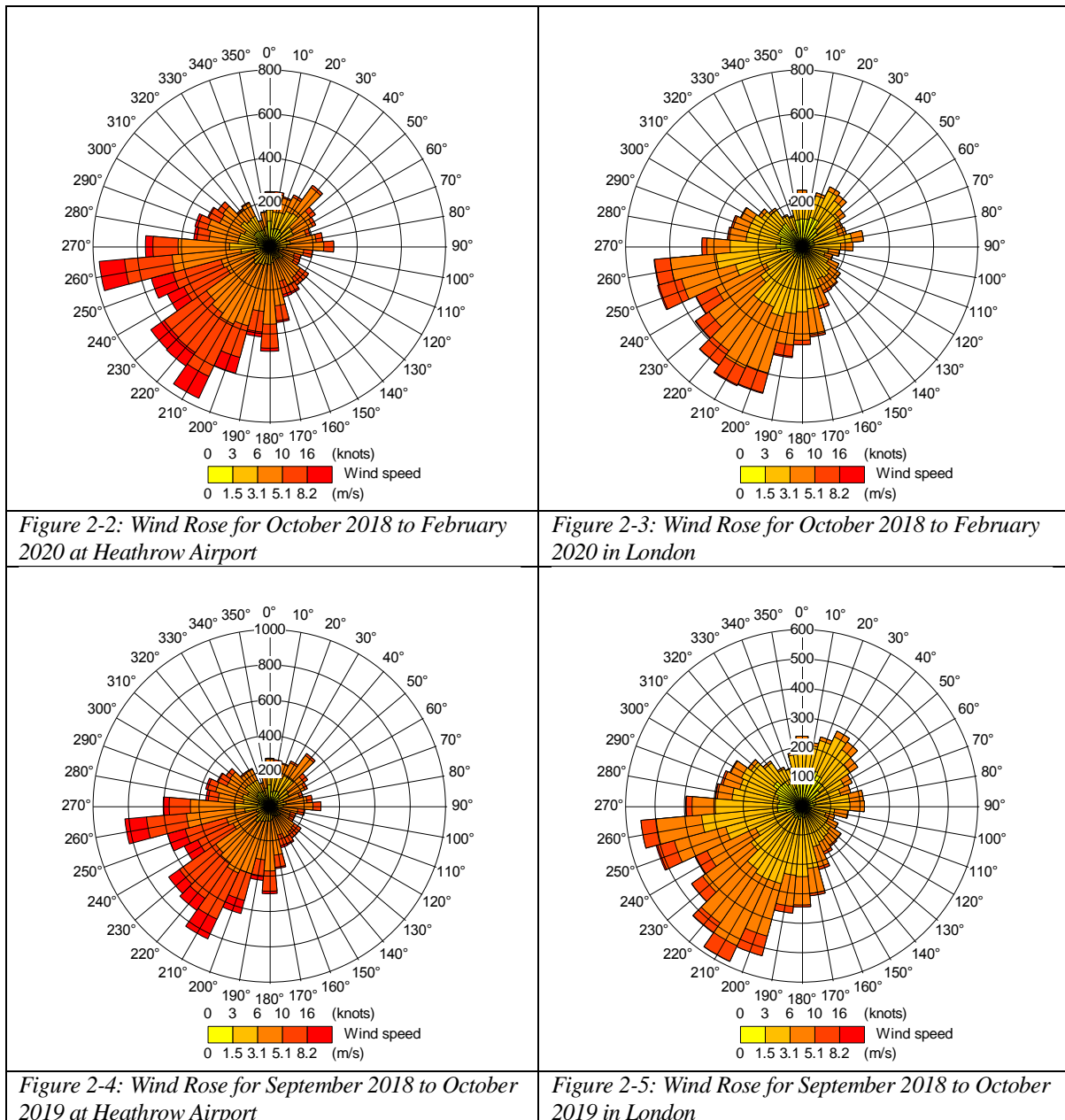


Figure 2-1 Diurnal emissions profiles used in modelling. Coloured lines show the weekday profiles for 17 road categories; black line shows the weekday profile used previously; the grey dotted lines show the profiles used for Saturday and Sunday, which are the same as used previously.

<sup>1</sup> Factor calculations for real world adjustments done by CERC based on the initial work done by: Carslaw, D and Rhys-Tyler, G 2013: New insights from comprehensive on-road measurements of NO<sub>x</sub>, NO<sub>2</sub> and NH<sub>3</sub> from vehicle emission remote sensing in London, UK. Atmos. Env. 81 pp 339–347.

## 2.1.2 Meteorology

The modelling uses hourly meteorological data collected at London Heathrow Airport. Two different periods were modelled. Static sites were modelled from 1 October 2018 to 29 February 2020. Mobile data locations were modelled from 1 September 2018 to 31 October 2019, to represent the drive period. Figure 2-2 to Figure 2-5 show the wind roses for the modelled periods at Heathrow Airport and as used as input to the ADMS-Urban model. The wind speeds are reduced in the built-up area of London due to the higher surface roughness compared with Heathrow airport, and there are small changes in wind direction.



## 2.1.3 Background

For NO<sub>x</sub>, NO<sub>2</sub>, PM<sub>10</sub>, PM<sub>2.5</sub> and Ozone, hourly background concentrations to represent the contribution from sources outside the modelled area were derived from 4 rural AURN

stations, that are located outside the M25, depending on which station was upwind at that hour. The AURN stations used for the background calculations are Chilbolton Observatory, Rochester Stoke, Lullington Heath and Wicken Fen. For PM10 and PM2.5, a maximum was imposed each hour that was the 5<sup>th</sup> percentile across all available LAQN and AQE reference monitors in London. For CO2, the rural DECC sites used were Ridge Hill, Tacolneston and Heathfield.

## **2.2 Measured data**

### **2.2.1 Static Measurement Sites**

#### **2.2.1.1 AQMesh**

Pre-scaled AQMesh data was downloaded for each station using the AirMonitors web API, at the highest frequency (1 minute for PM<sub>2.5</sub> and 15 minutes for NO<sub>2</sub> before the 5<sup>th</sup> April 2019 and 1 minute after). Any data points flagged as invalid were redacted before applying pollutant and station-specific scaling factors, which have been calculated using one of three different methods: colocation with a reference monitor, colocation with a gold standard pod or calibrated using baselines extracted across the entire pod network. All scaling factors for PM<sub>2.5</sub> were calculated using the network calibration method. After applying scaling factors, any negative concentrations were redacted before hourly averages were calculated using a data validity threshold of 85%. Finally, the hourly average NO<sub>2</sub> values were converted from ppb to µg/m<sup>3</sup> for comparison with model values. All AQMesh data is provisional at this stage.

#### **2.2.1.2 LAQN**

Hourly average data for NO<sub>2</sub> and PM<sub>2.5</sub> at each station in the LAQN network was downloaded using the importKCL() openair function in R. For PM<sub>2.5</sub>, any hourly means above 500 µg/m<sup>3</sup> were redacted. The data is ratified for the majority of stations up until 30<sup>th</sup> January 2019 and provisional otherwise.

#### **2.2.1.3 AQE**

Hourly average data for NO<sub>2</sub> and PM<sub>2.5</sub> at each station in the AQE network was downloaded using the importAQE() openair function in R. The API does not cover the AURN sites that are controlled by AQE and these must be downloaded separately using the importAURN() openair function in R. For PM<sub>2.5</sub>, any hourly mean values above 500 µg/m<sup>3</sup> were redacted. The data is ratified for the majority of stations up until 30<sup>th</sup> January 2019 and provisional otherwise.

### **2.2.2 Mobile measurements**

The mobile measurements are downloaded from the aggregated 30m dataset (QAQC version 7) in the Street View Air Quality London data store in Google Big Query. The dataset contained the median of all valid 1-second measurements from 2 cars along a 30m road segment, for each 1-hour time window the cars were driving.

## 3. Results

### 3.1 Static sites

Static sites have been represented in the model as discrete receptors with the appropriate position and height. All explicit roads within 500m of a receptor are modelled explicitly as road sources; remaining emissions are aggregated into 1km grid cells. AQMesh, LAQN and AQE sites have been modelled for the period 1 October 2018 to 29 February 2020, to avoid the period affected by COVID-19. Time series plots for NOX, NO2, PM10 and PM2.5 comparing network-averaged hourly modelled and measured concentrations for the period of the analysis is shown in Figure 3-1.

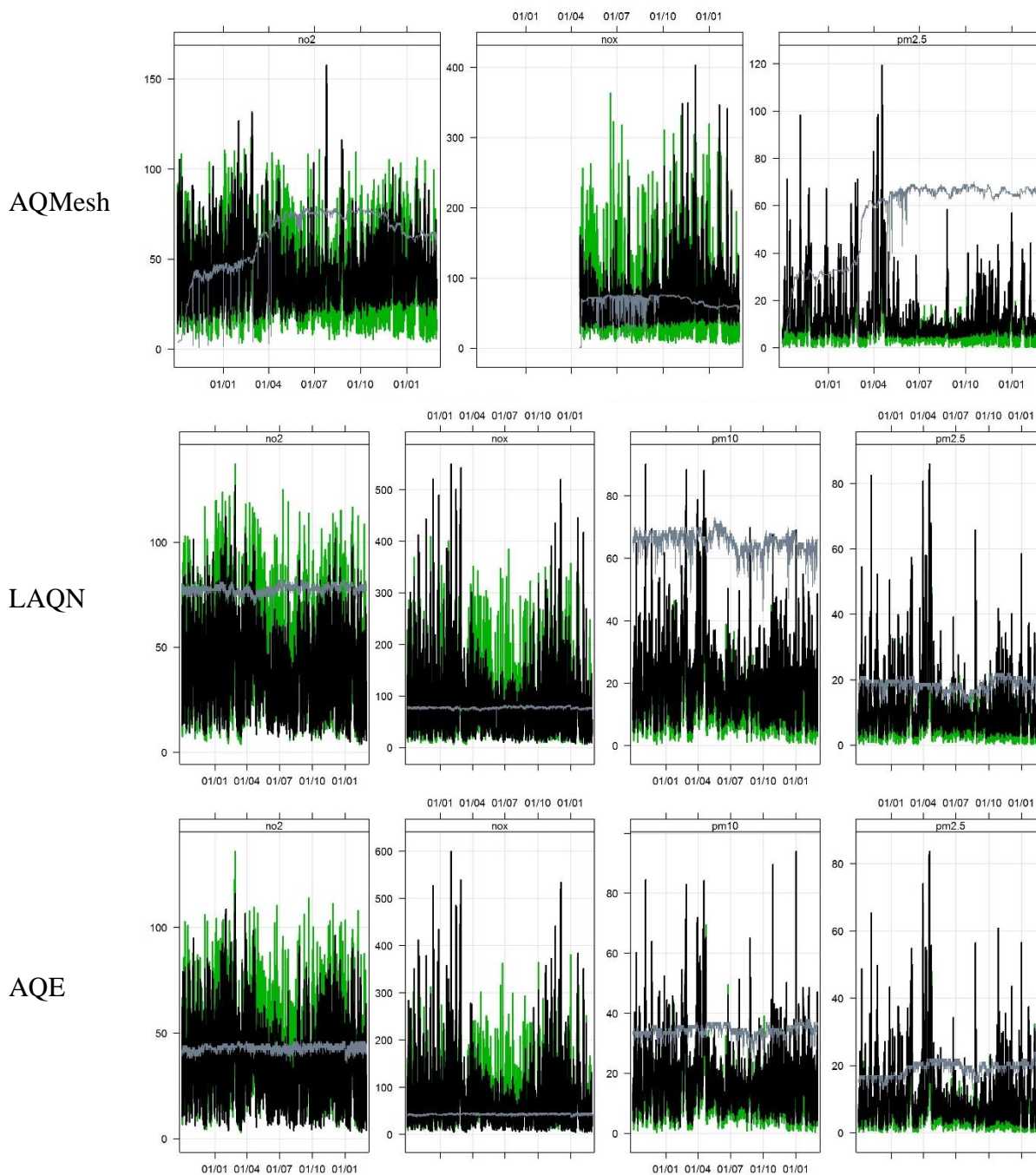


Figure 3-1 Time plots of hourly concentration averaged over all sites in each network. In each case, the black line represents the measured concentration and the green line represents the modelled concentration ( $\mu\text{g}/\text{m}^3$ ). The grey line represents the number of sites included in the average. The period covered is 1 October 2018 to 29 February 2020.

Overall model verification statistics for NO<sub>2</sub>, PM<sub>10</sub>, PM<sub>2.5</sub> and Ozone are given in Table 3-1; overall time variation profiles for NO<sub>x</sub> at all sites are given in Figure 3-2. The verification statistics show that the model shows good agreement for NO<sub>2</sub> at LAQN and AQE sites but has a negative bias at AQMesh sites; this is likely to be due to issues with the AQMesh NO<sub>2</sub> sensors not detecting low levels of NO<sub>2</sub>, and upward drift in the NO<sub>2</sub> sensors. PM<sub>10</sub> and PM<sub>2.5</sub> have a negative bias at all sites, which the figures show is likely to be partly due to the background concentrations being underestimated. These have been calculated using the 5<sup>th</sup> percentile of local measurements as an upper limit on the background PM levels; this method will be improved for the next round of modelling (D5.1). The modelled diurnal NO<sub>x</sub> profiles for all site types show three particular features: the morning and evening peaks are slightly too early in the modelled results; the modelled morning peak is too high; and modelled concentrations at weekends are too high, particularly on Sunday evenings. These anomalies should be addressed for the next round of modelling.

Pollutant	Network	Number of Sites	Number of Valid Values	Obs Mean $\mu\text{g}/\text{m}^3$	Mod Mean $\mu\text{g}/\text{m}^3$	MB $\mu\text{g}/\text{m}^3$	NMSE	R	FAC2
<b>NO<sub>2</sub></b>	AQE	46	540866	35.3	35.3	0.0	0.29	0.68	0.80
<b>NO<sub>2</sub></b>	AQMESH	97	760627	40.3	34.5	-5.8	0.36	0.50	0.75
<b>NO<sub>2</sub></b>	LAQN	83	966654	40.4	39.0	-1.4	0.32	0.64	0.79
<b>NO<sub>x</sub></b>	AQE	46	540870	73.5	65.9	-7.6	0.86	0.64	0.70
<b>NO<sub>x</sub></b>	AQMESH	84	508654	70.1	60.6	-9.5	0.77	0.51	0.67
<b>NO<sub>x</sub></b>	LAQN	83	961665	88.1	80.0	-8.1	0.89	0.59	0.70
<b>PM<sub>2.5</sub></b>	AQE	24	239670	10.2	7.7	-2.5	0.41	0.85	0.77
<b>PM<sub>2.5</sub></b>	AQMESH	73	671961	11.8	7.6	-4.2	0.93	0.73	0.69
<b>PM<sub>2.5</sub></b>	LAQN	22	232675	11.7	8.4	-3.2	0.44	0.84	0.75
<b>PM<sub>10</sub></b>	LAQN	74	813420	20.4	14.7	-5.7	0.49	0.68	0.79
<b>PM<sub>10</sub></b>	AQE	39	427756	17.7	13.7	-4.1	0.35	0.76	0.84
<b>Ozone</b>	LAQN	16	172102	33.8	38.1	4.3	0.25	0.74	0.66
<b>Ozone</b>	AQE	8	90353	35.3	38.7	3.4	0.22	0.76	0.68

Table 3-1 Summary statistics for modelled and observed hourly mean concentrations ( $\mu\text{g}/\text{m}^3$ ) for each monitoring network. MB = Mean bias; NMSE = Normalised mean square error; R = correlation coefficient; FAC2 = percentage of modelled data points within a fraction of 2 of the measured value.

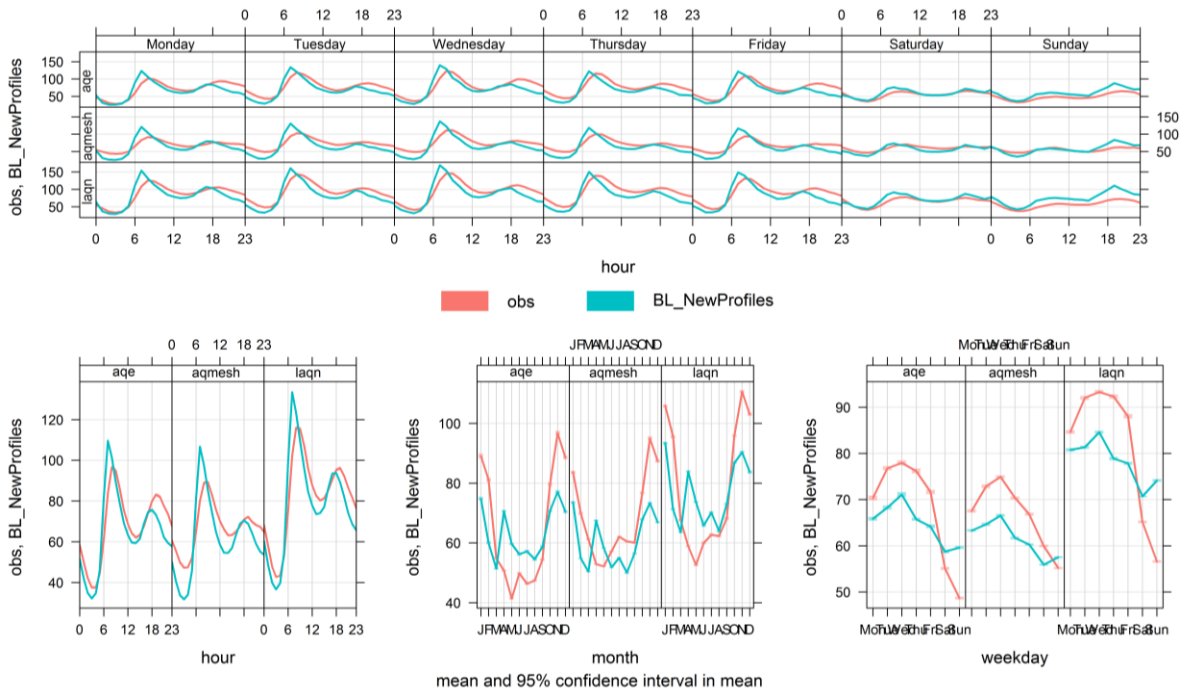


Figure 3-2 Time Variation plot of observed (orange) and modelled (blue) NOX (ug/m<sup>3</sup>) by network. The top plot shows the diurnal profile over 7 days, the bottom left plot shows the average diurnal profile for each network, the bottom middle plot shows the monthly variation and the bottom right plot shows the variation by day of the week.

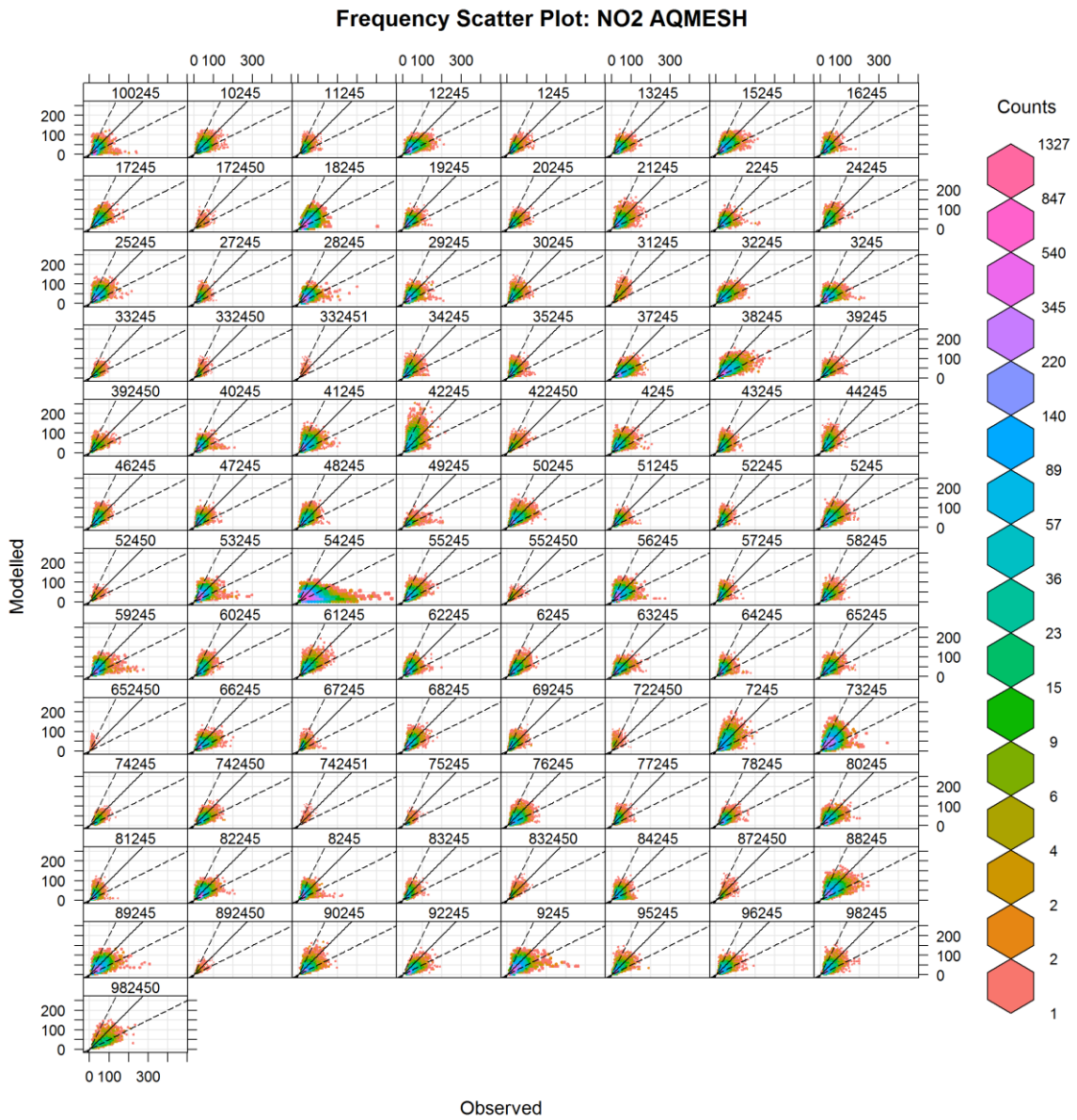


Figure 3-3 Frequency scatter plots comparing modelled and observed hourly concentrations of NO<sub>2</sub> (ug/m<sup>3</sup>) for each AQMesh site.

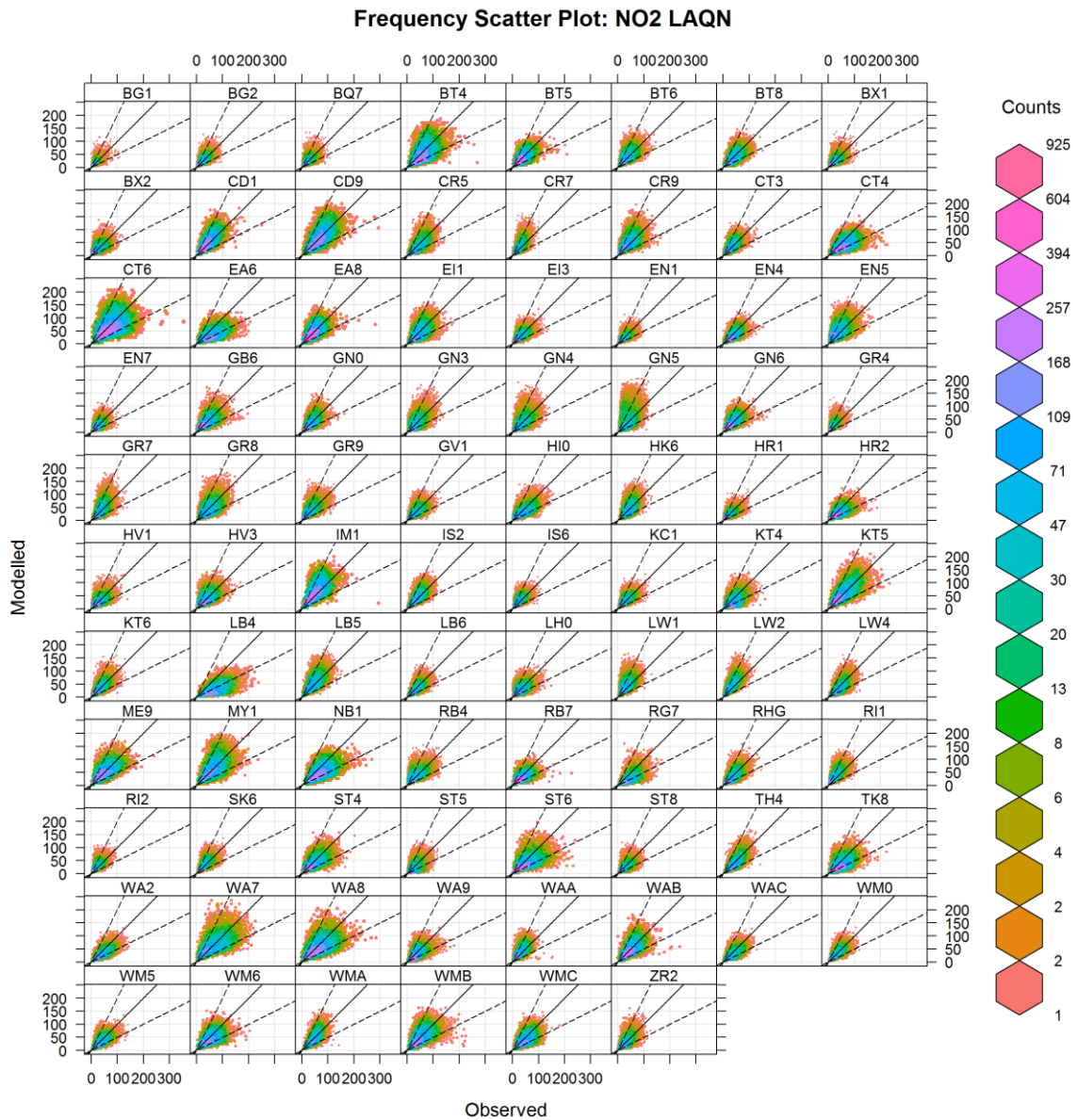


Figure 3-4 Frequency scatter plots comparing modelled and observed hourly concentrations of NO<sub>2</sub> ( $\mu\text{g}/\text{m}^3$ ) for each LAQN site.

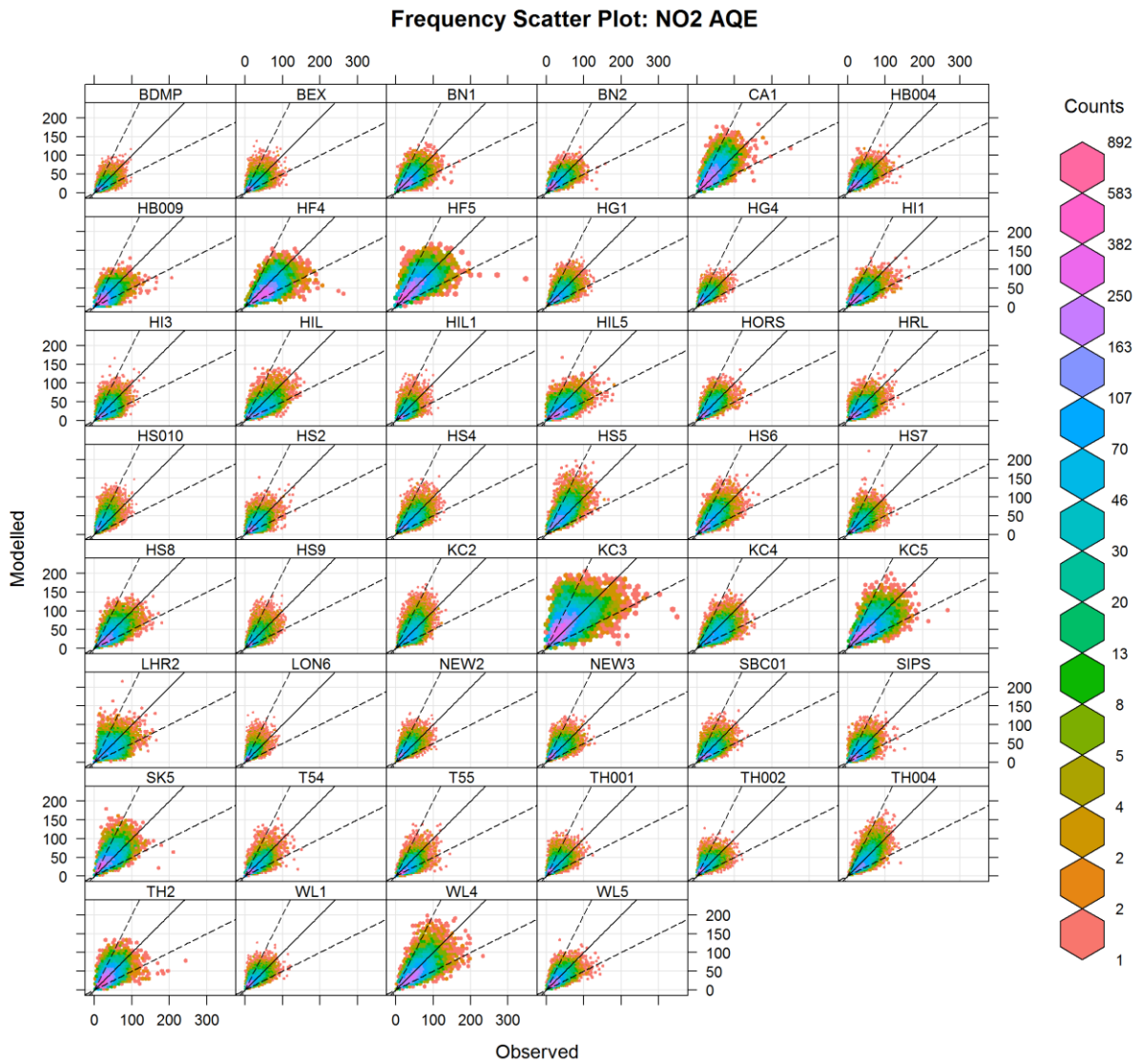


Figure 3-5 Frequency scatter plots comparing modelled and observed hourly concentrations of NO<sub>2</sub> (ug/m<sup>3</sup>) for each AQE site.

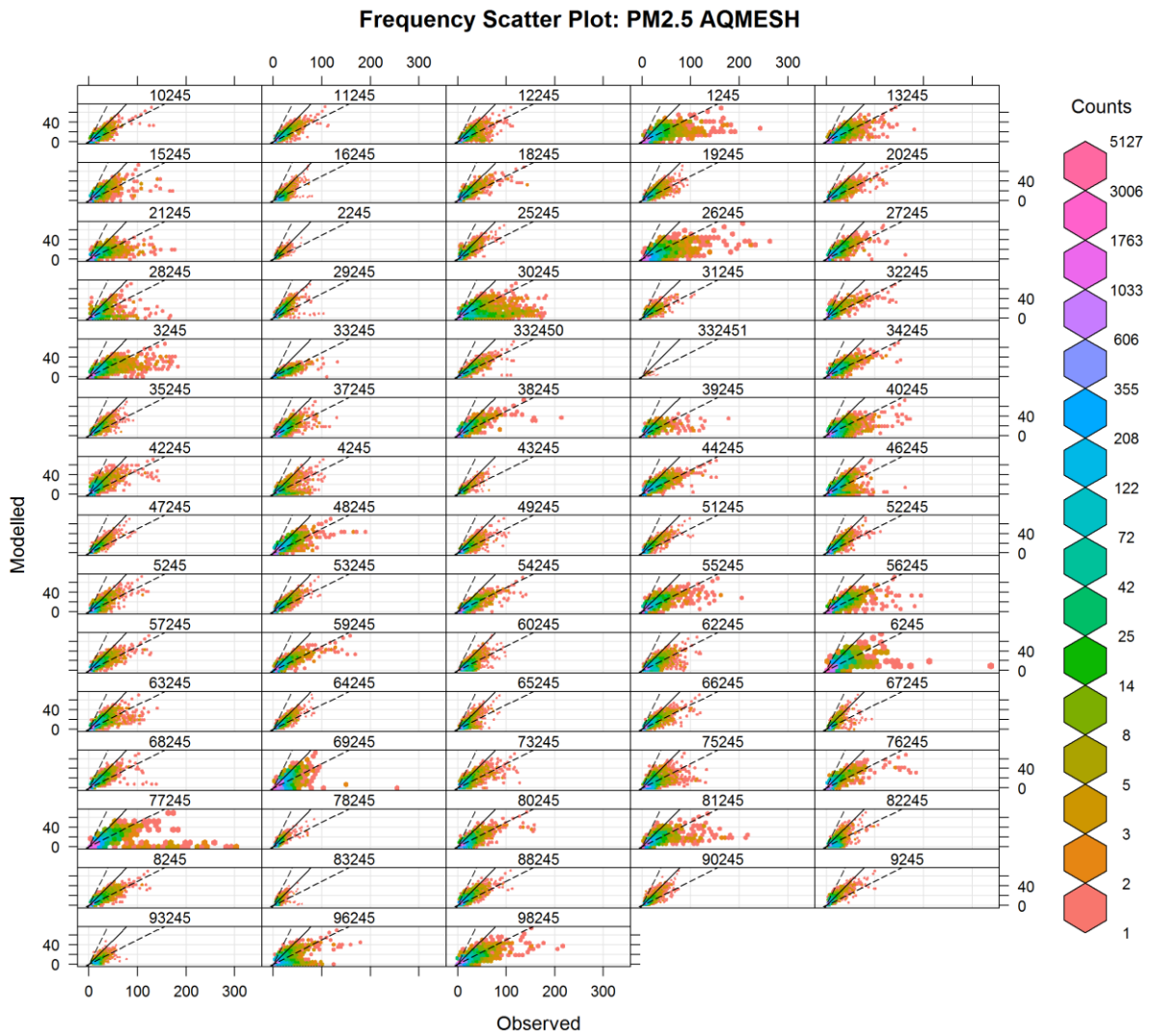


Figure 3-6 Frequency scatter plots comparing modelled and observed hourly concentrations of PM2.5 (ug/m3) for each AQMesh site.

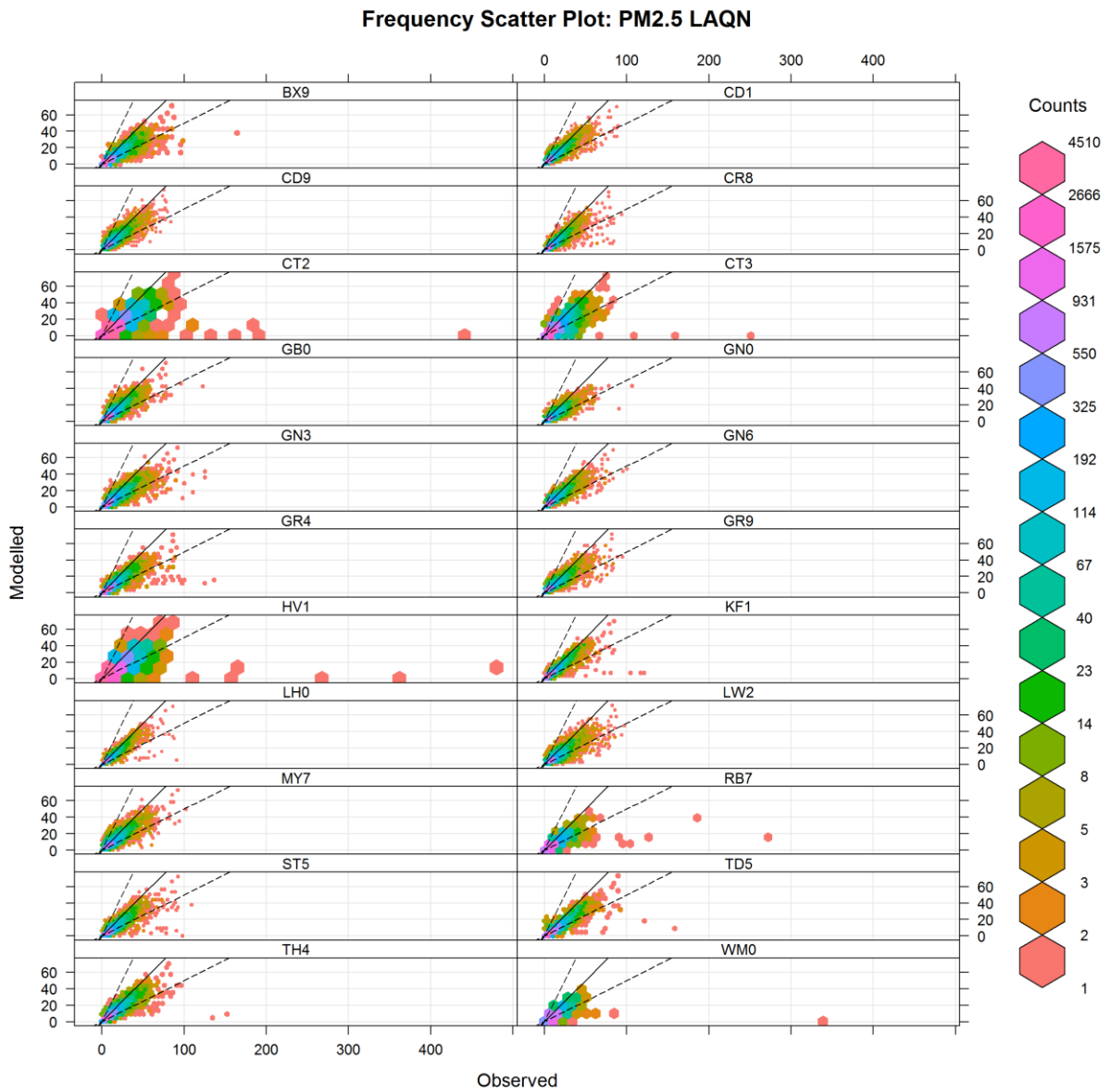


Figure 3-7 Frequency scatter plots comparing modelled and observed hourly concentrations of PM2.5 ( $\mu\text{g}/\text{m}^3$ ) for each LAQN site.

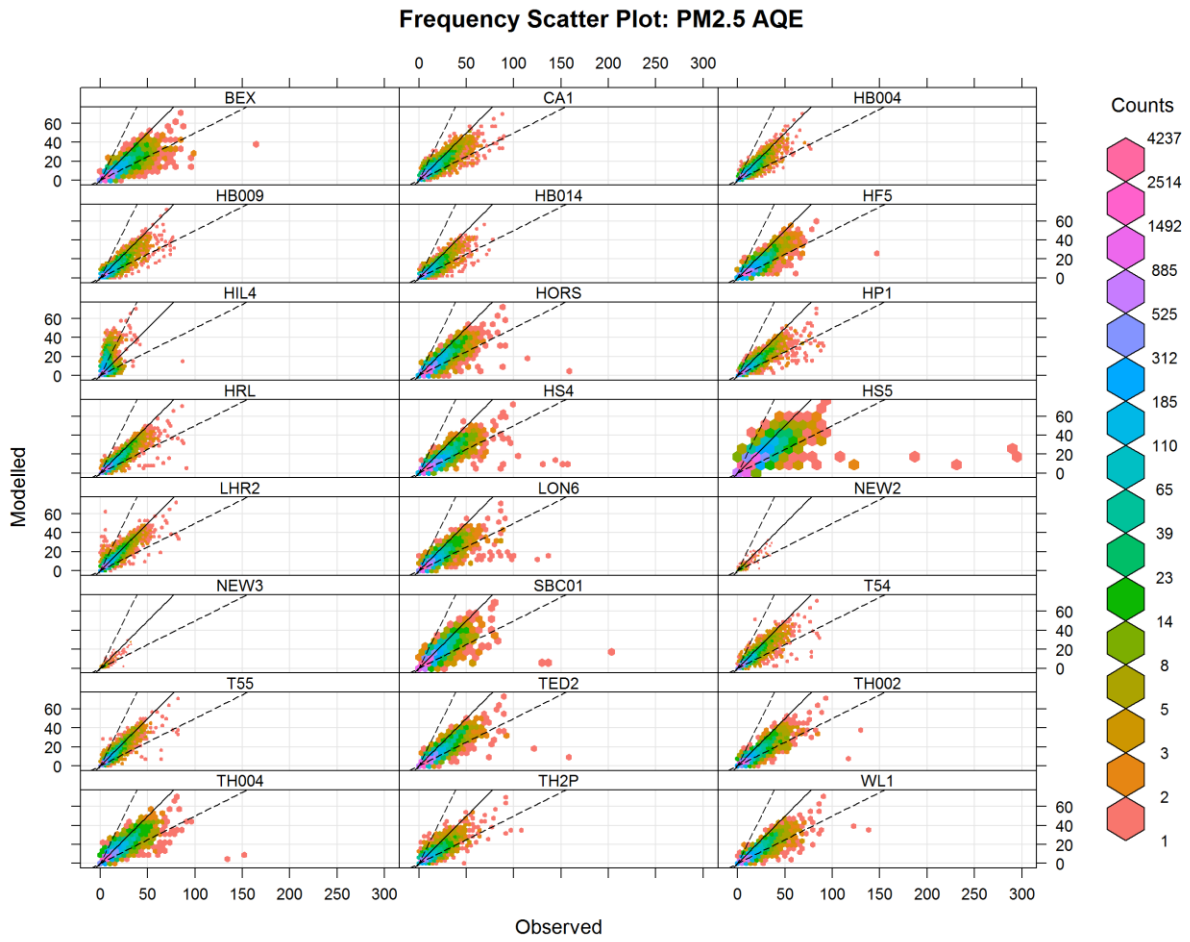


Figure 3-8 Frequency scatter plots comparing modelled and observed hourly concentrations of PM<sub>2.5</sub> ( $\mu\text{g}/\text{m}^3$ ) for each AQE site.

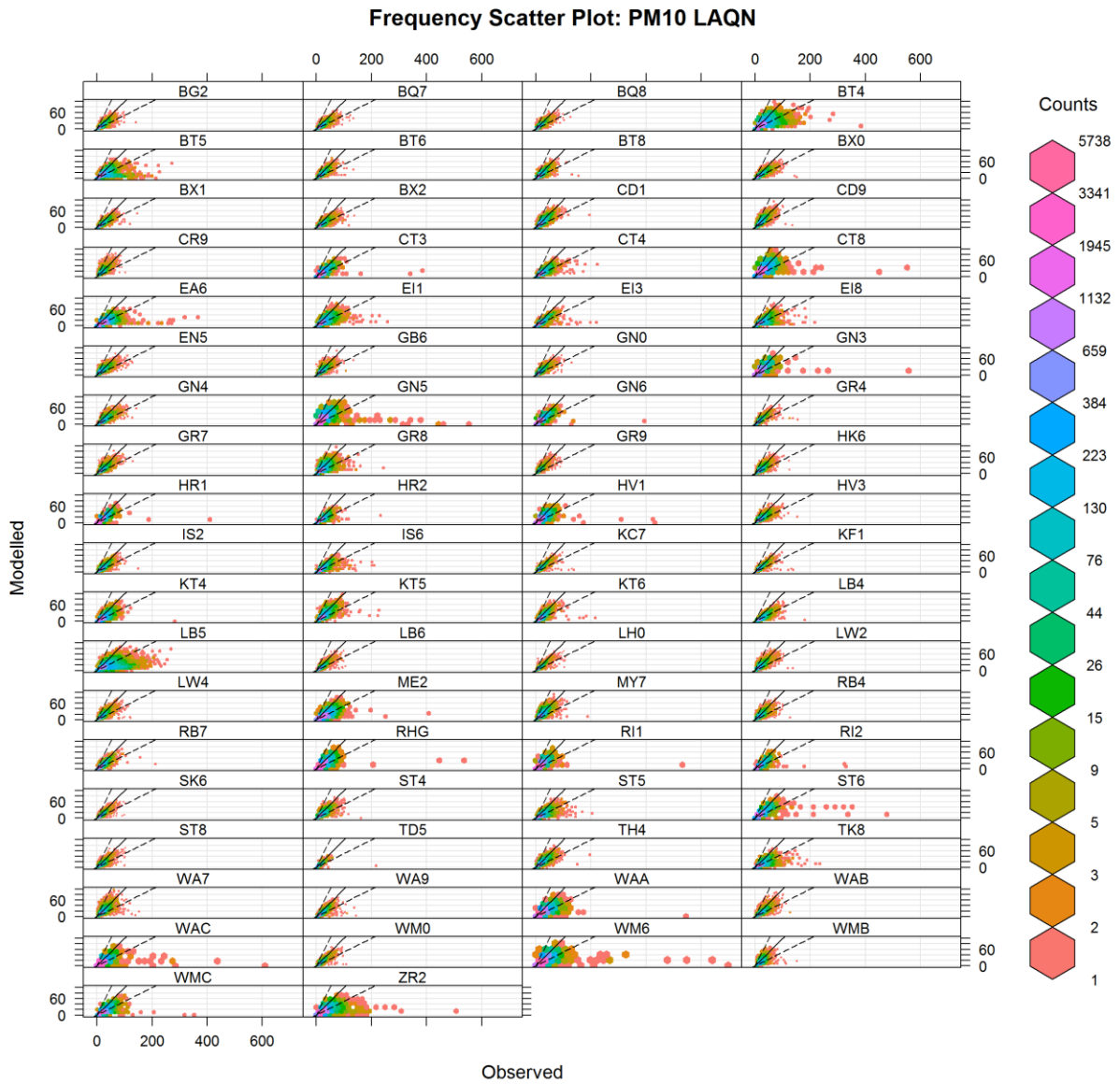


Figure 3-9 Frequency scatter plots comparing modelled and observed hourly concentrations of PM10 (ug/m3) for each LAQN site.

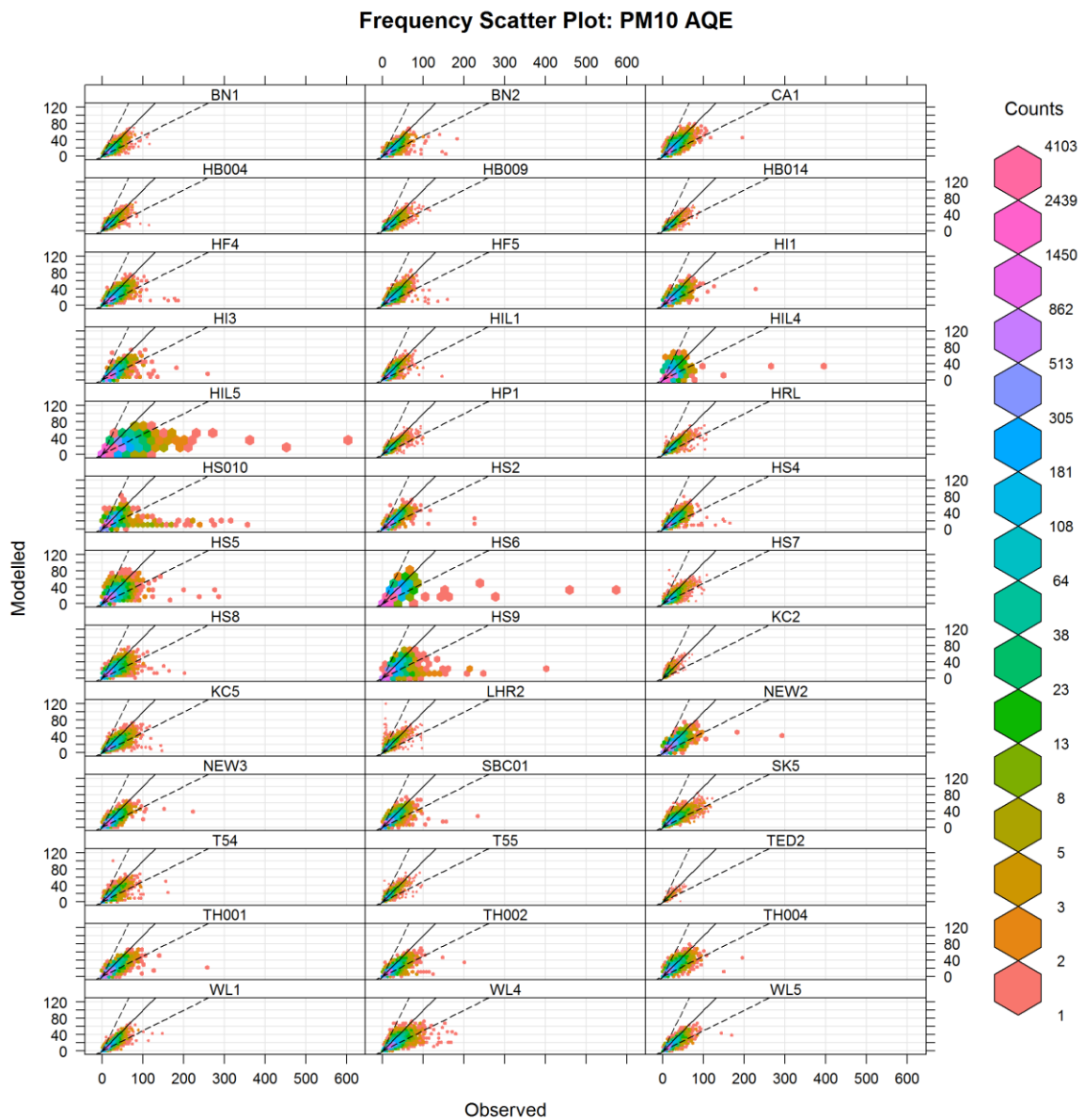


Figure 3-10 Frequency scatter plots comparing modelled and observed hourly concentrations of PM10 ( $\mu\text{g}/\text{m}^3$ ) for each AQE site.

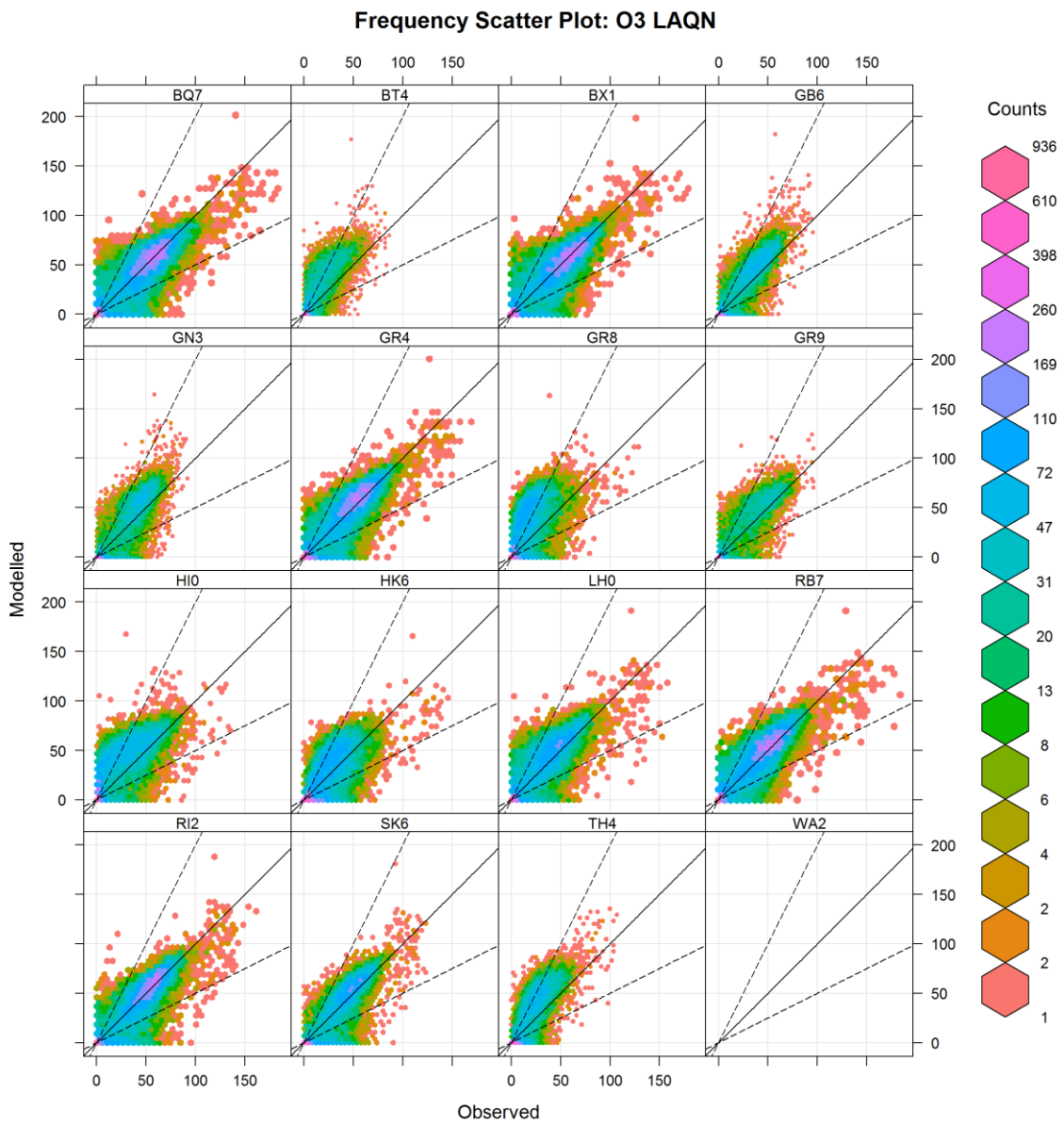


Figure 3-11 Frequency scatter plots comparing modelled and observed hourly concentrations of Ozone ( $\mu\text{g}/\text{m}^3$ ) for each LAQN site.

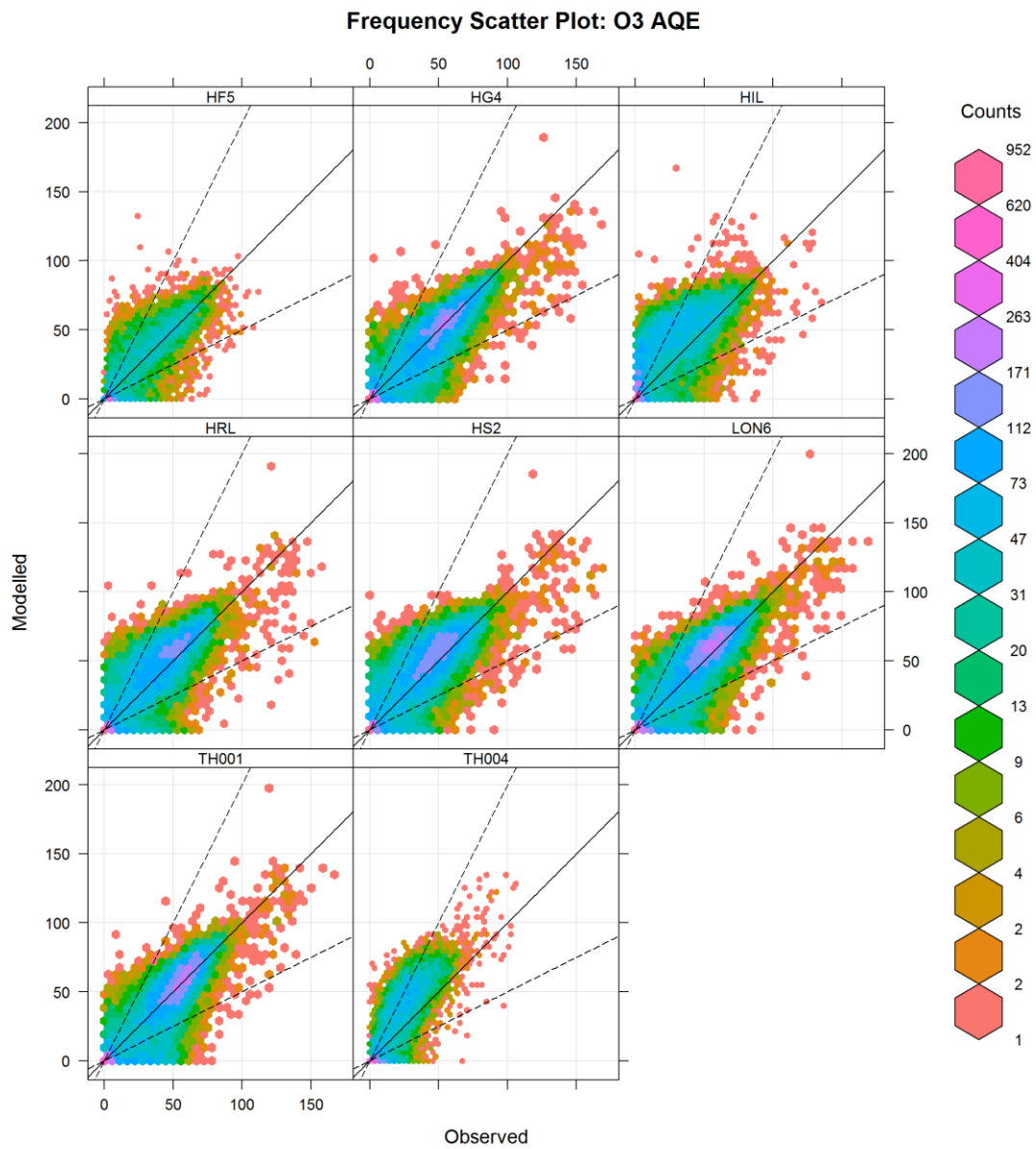


Figure 3-12 Frequency scatter plots comparing modelled and observed hourly concentrations of Ozone ( $\mu\text{g}/\text{m}^3$ ) for each AQE site.

## 3.2 Mobile locations

Mobile measurements have been represented in the model by placing discrete receptors at points along the road centrelines, for roads that have been driven by the Google Cars and are included in the LAEI. Each receptor has been assigned to a 30m road segment for the calculation of hourly and period averages per road segment. All receptors were assumed to 1.5m above the ground to accurately reflect the inlet height on the Google Cars. The model calculates hourly averages from 1<sup>st</sup> September 2018 to 31<sup>st</sup> October 2019, and then only the hourly values for hours in which there are valid Google car measurements are extracted for comparison. Hourly values at these receptors have been aggregated to the same 30m segments as the measured data, and average values have been calculated for each segment.

Figure 3-13 and Table 3-2 compare the modelled and measured average values on each 30m road segment, where only driven hours are included in the average. Interpretation of these comparisons should be done with care, because the modelled data represents an average of hourly averages, whereas measured values may represent only a small number of 1 second measurements within the hour. Agreement is generally reasonably good but with a negative bias for NO<sub>x</sub>, NO<sub>2</sub> and CO<sub>2</sub>. The peak measured concentrations are higher than the modelled concentrations is to be expected because of the much shorter averaging time for the measurements. The model has reasonable agreement for PM<sub>2.5</sub> whilst overestimating PM<sub>10</sub>; this may be caused by a higher level of uncertainty in the mobile PM<sub>10</sub> measurements. Figure 3-14 through to Figure 3-19 provide equivalent maps of measured and modelled concentrations at mobile locations.

Pollutant	Number of road segments	Observed mean	Modelled mean	MB	FAC2	R	RMSE
<b>NO<sub>2</sub></b>	40121	70.6	57.1	-13.5	0.85	0.46	40.3
<b>NO<sub>x</sub></b>	32222	234.3	142.5	-91.8	0.65	0.38	222.1
<b>PM<sub>10</sub></b>	32669	12.8	19.0	6.2	0.69	0.36	12.2
<b>PM<sub>2.5</sub></b>	32665	10.0	10.3	0.4	0.92	0.64	5.1
<b>CO<sub>2</sub></b>	42530	449.9	410.8	-39.4	1.00	0.43	48.8
<b>O<sub>3</sub></b>	37694	32.0	34.0	2.0	0.81	0.75	12.8

Table 3-2 Statistics comparing modelled and observed concentrations aggregated into 30m road segments and averaged over the whole period. MB = Mean Bias; FAC2 = fraction within a factor of 2 of the observed; R = Correlation Coefficient; RMSE = root-mean-square error. Units are ug/m<sup>3</sup> for all pollutants except CO<sub>2</sub> which is ppm.

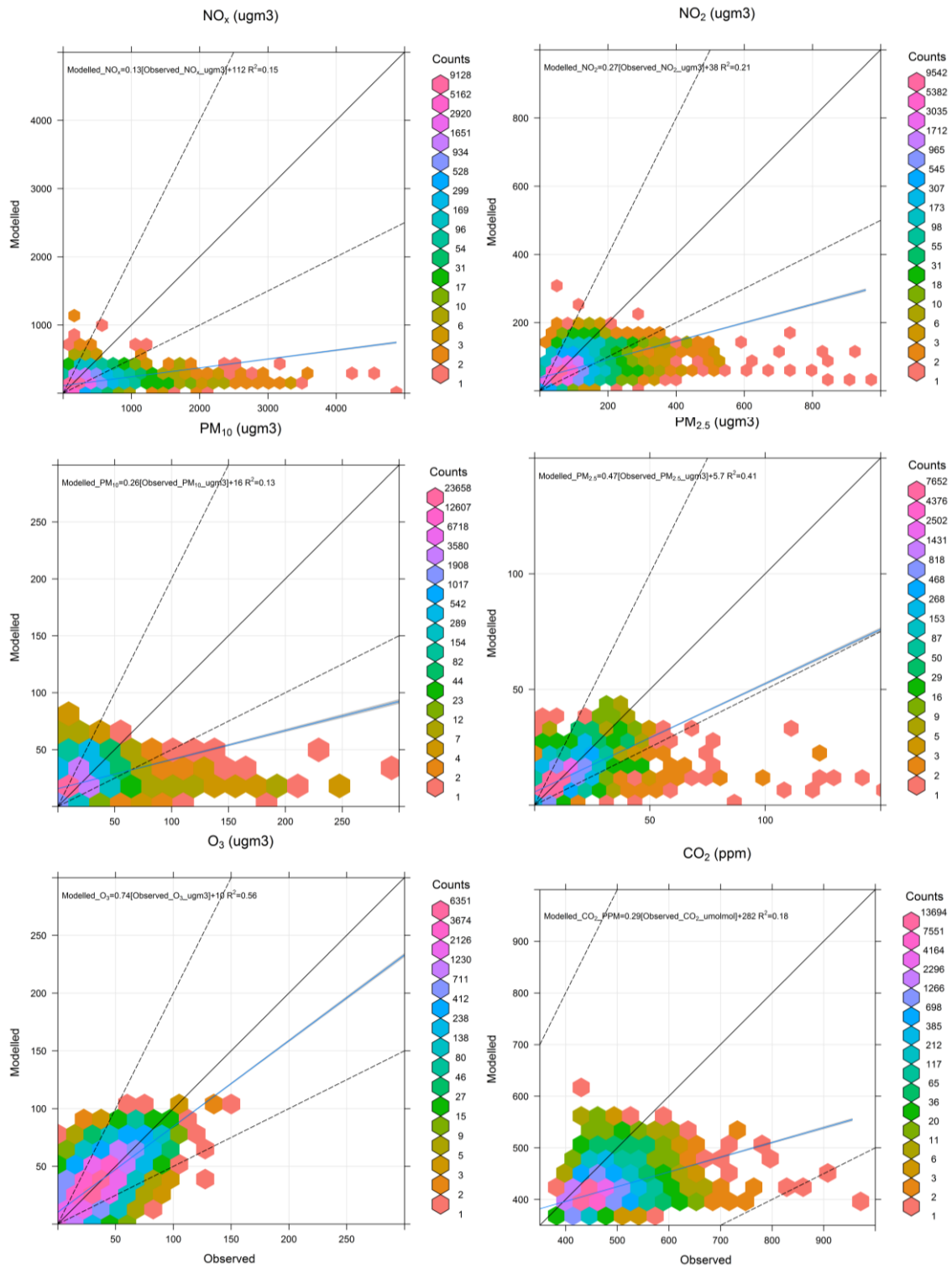


Figure 3-13 Frequency scatter plots comparing modelled and observed results aggregated into 30m road segments and averaged over the whole period. Only hours and road segments driven and modelled are included.

### 3.2.1 NOX

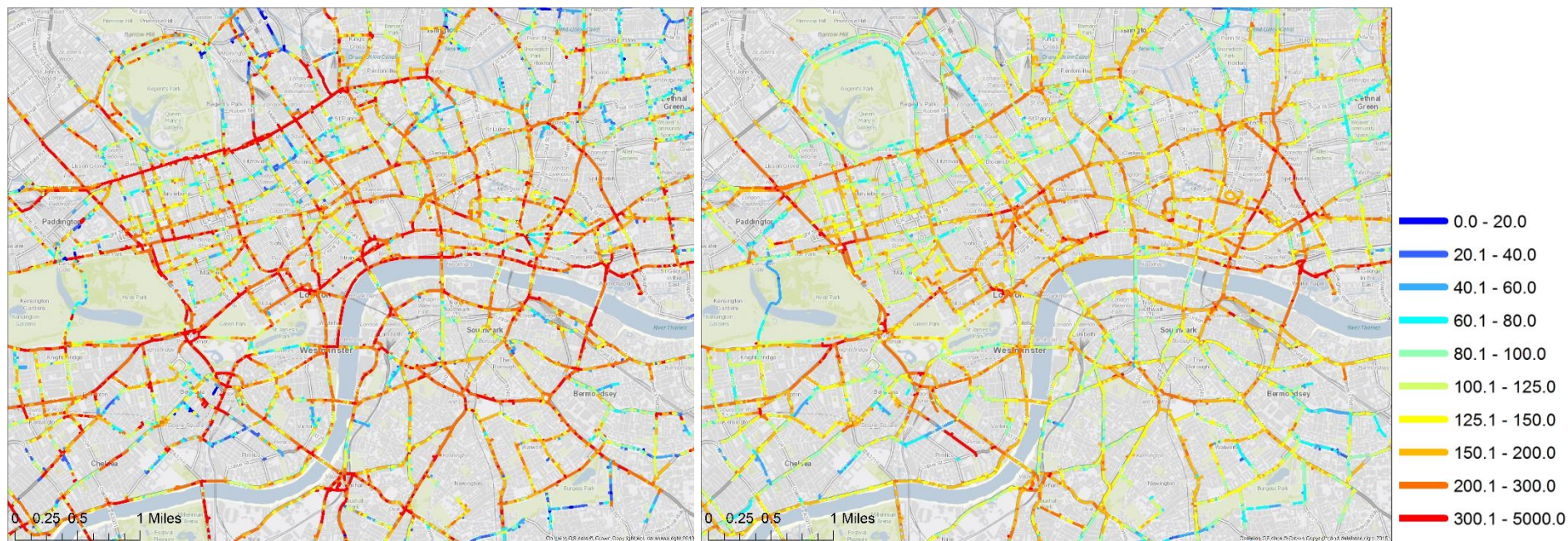


Figure 3-14 Observed (left) and modelled (right) NOX ( $\mu\text{g}/\text{m}^3$ ), showing only those roads that were driven and modelled, aggregated to 30m road segments. The modelled average for each road segment only includes hours that were driven for that road segment.

### 3.2.2 NO2

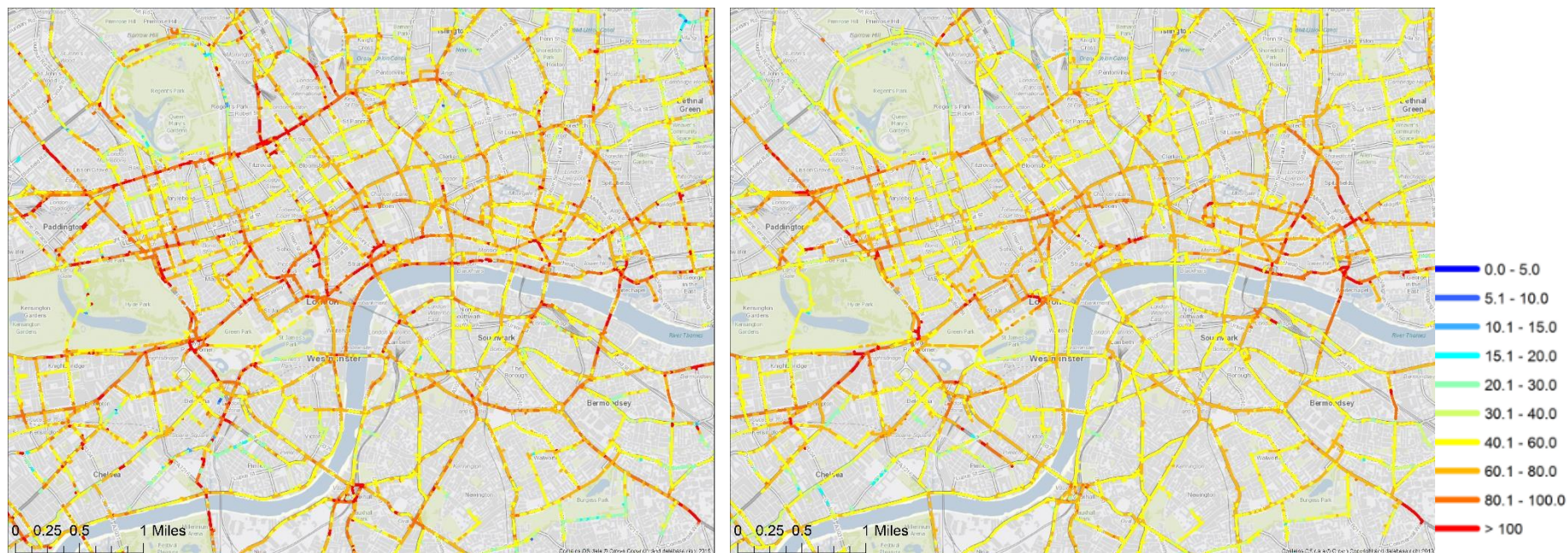


Figure 3-15 Observed (left) and modelled (right) NO<sub>2</sub> ( $\mu\text{g}/\text{m}^3$ ), showing only those roads that were driven and modelled, aggregated to 30m road segments. The modelled average for each road segment only includes hours that were driven for that road segment.

### 3.2.3 PM10

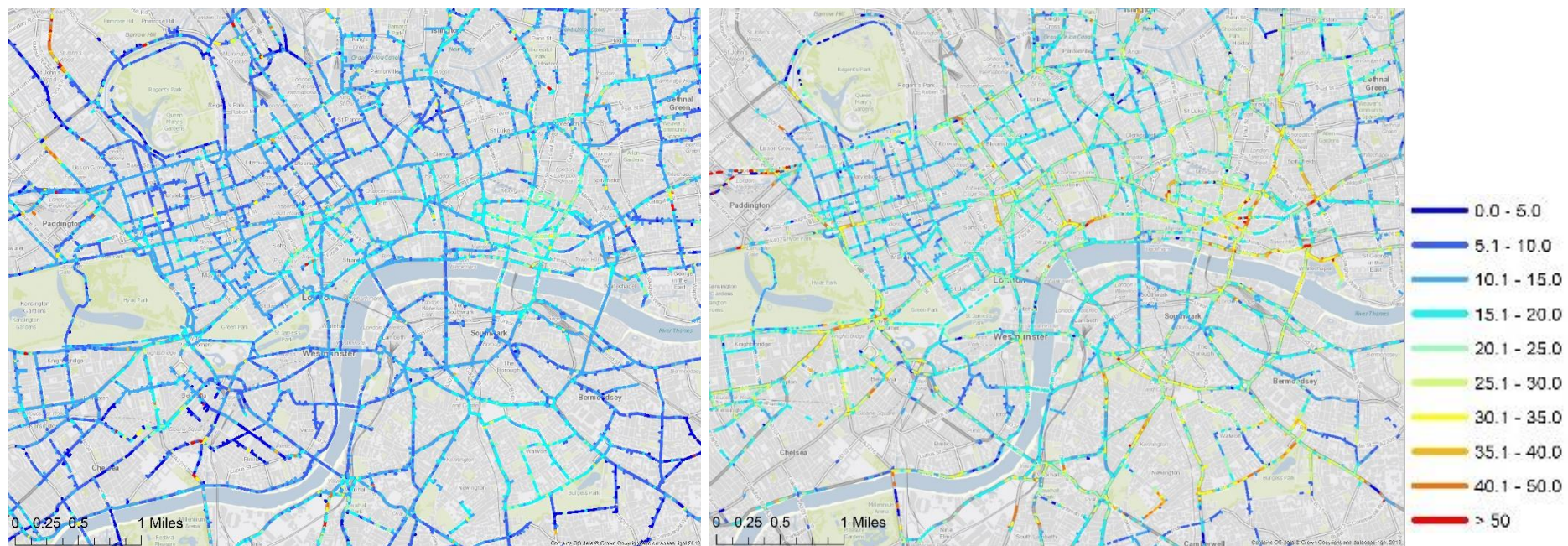


Figure 3-16 Observed (left) and modelled (right) PM10 ( $\mu\text{g}/\text{m}^3$ ), showing only those roads that were driven and modelled, aggregated to 30m road segments. The modelled average for each road segment only includes hours that were driven for that road segment.

### 3.2.4 PM2.5



Figure 3-17 Observed (left) and modelled (right) PM2.5 ( $\mu\text{g}/\text{m}^3$ ), showing only those roads that were driven and modelled, aggregated to 30m road segments. The modelled average for each road segment only includes hours that were driven for that road segment.

### 3.2.5 Ozone

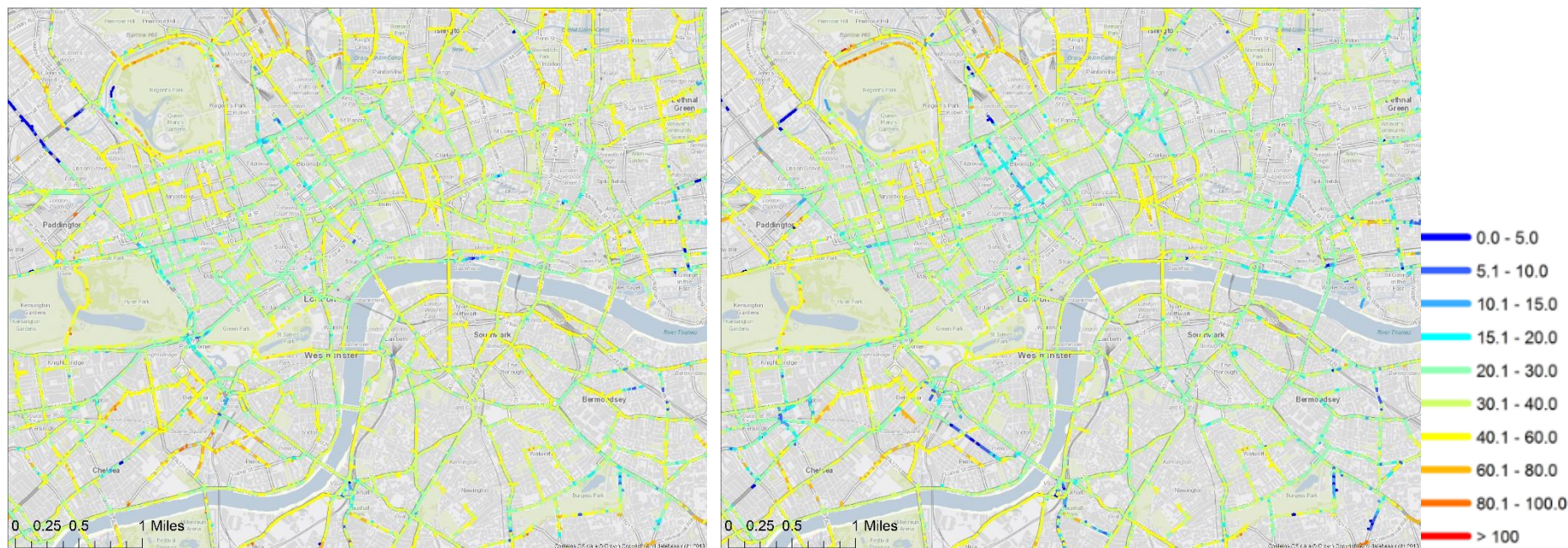


Figure 3-18 Observed (left) and modelled (right) Ozone ( $\mu\text{g}/\text{m}^3$ ), showing only those roads that were driven and modelled, aggregated to 30m road segments. The modelled average for each road segment only includes hours that were driven for that road segment.

### 3.2.6 CO2

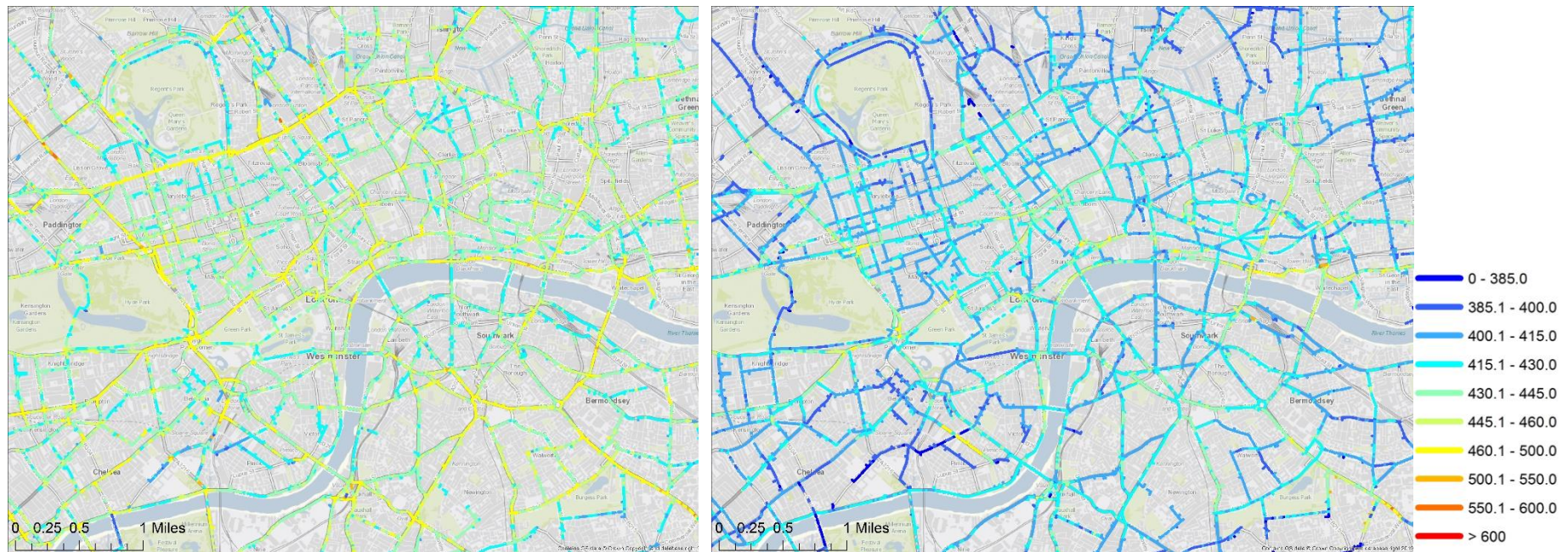


Figure 3-19 Observed (left) and modelled (right) CO<sub>2</sub> (ppm), showing only those roads that were driven and modelled, aggregated to 30m road segments. The modelled average for each road segment only includes hours that were driven for that road segment.

### 3.3 Mobile Locations – Continuous Modelling

The previous section presented maps of average modelled concentrations that only included the hours that were driven on each segment. In this section we present maps of average modelled concentration for each 30m road segment for each driven road for the whole period of the Google Car drives: 1 September 2018 to 31 October 2019.

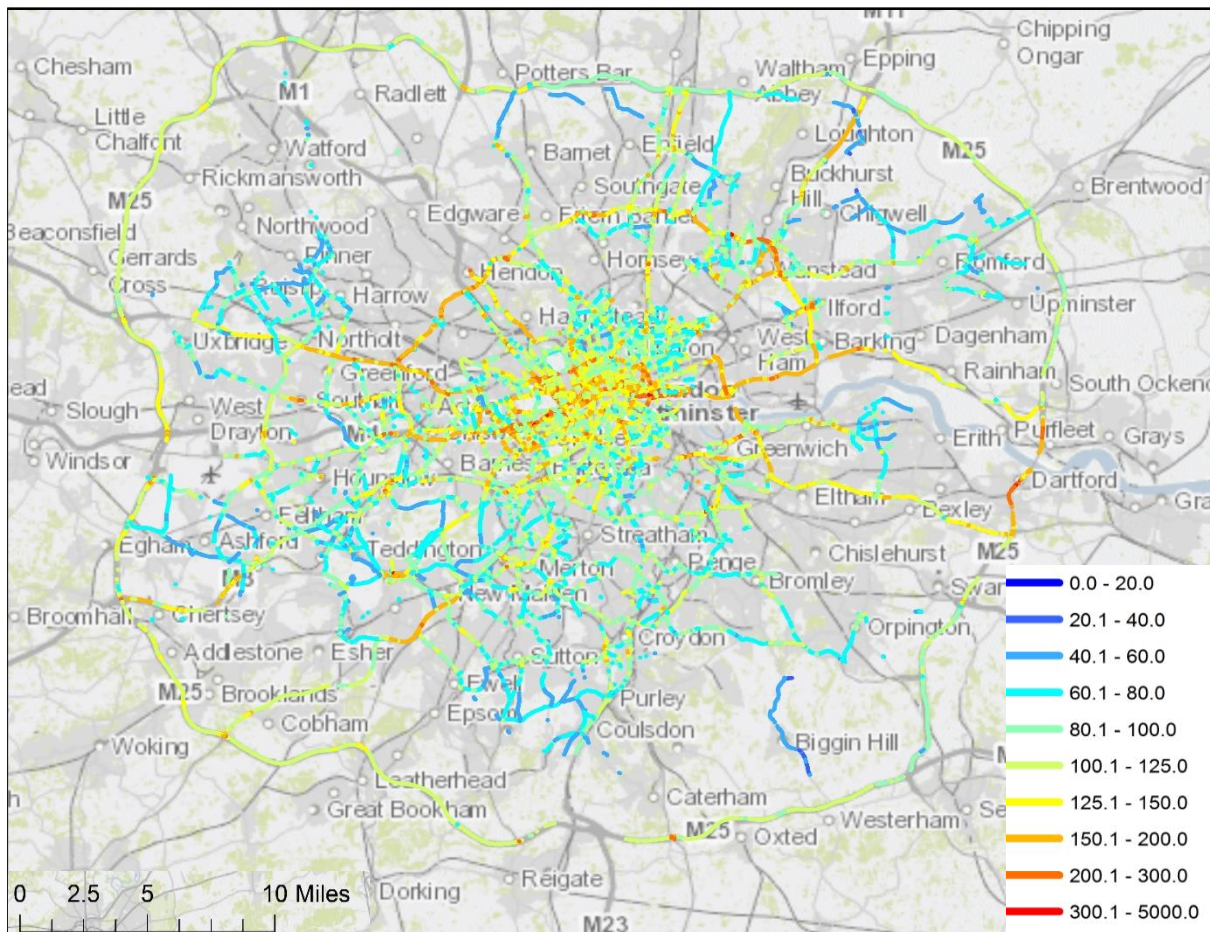


Figure 3-20 Period average modelled NOx concentration (ug/m3) for each 30m driven road segment for the period 1 September 2018 to 31 October 2019.

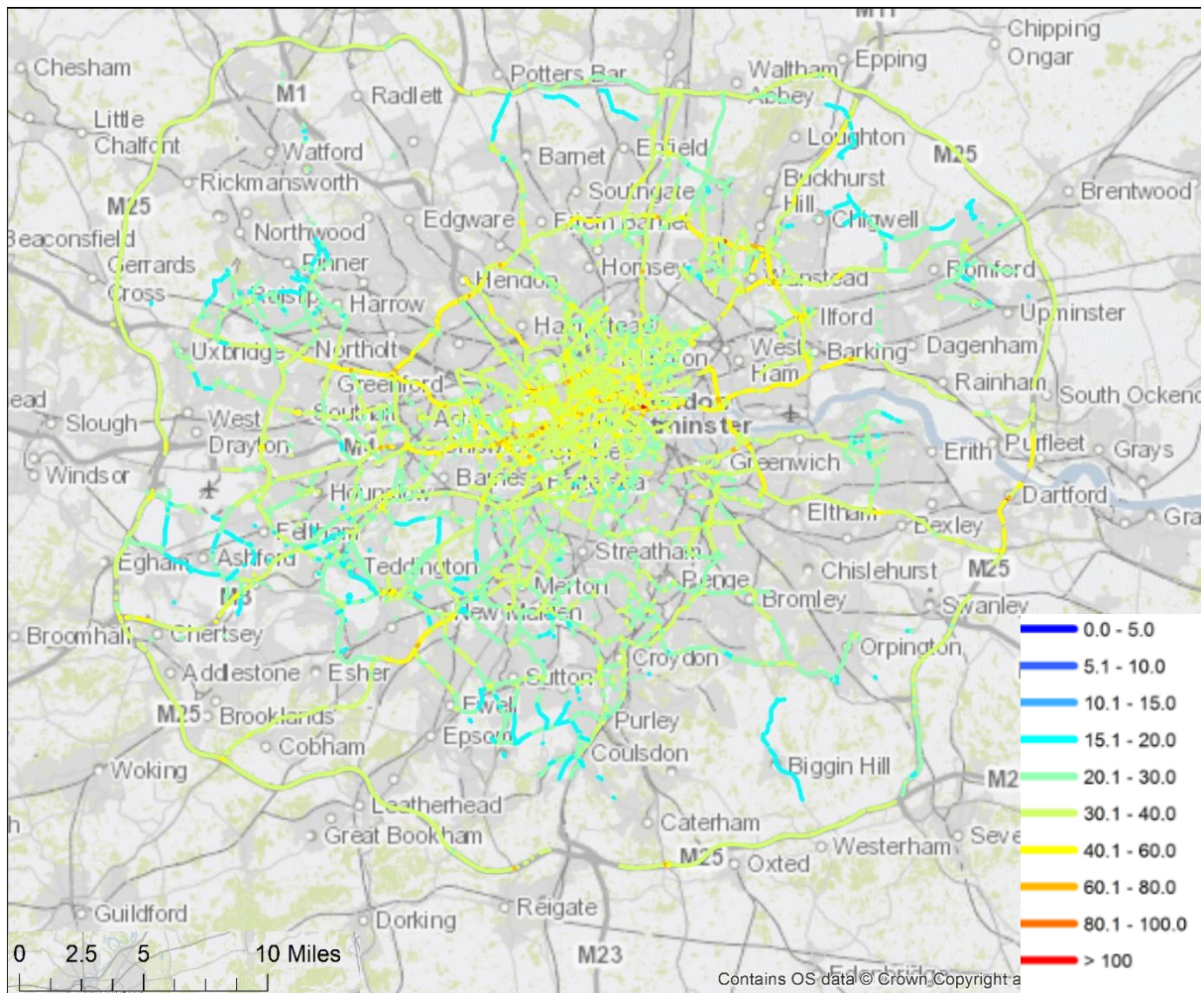


Figure 3-21 Period average modelled NO<sub>2</sub> concentration (ug/m<sup>3</sup>) for each 30m driven road segment for the period 1 September 2018 to 31 October 2019.

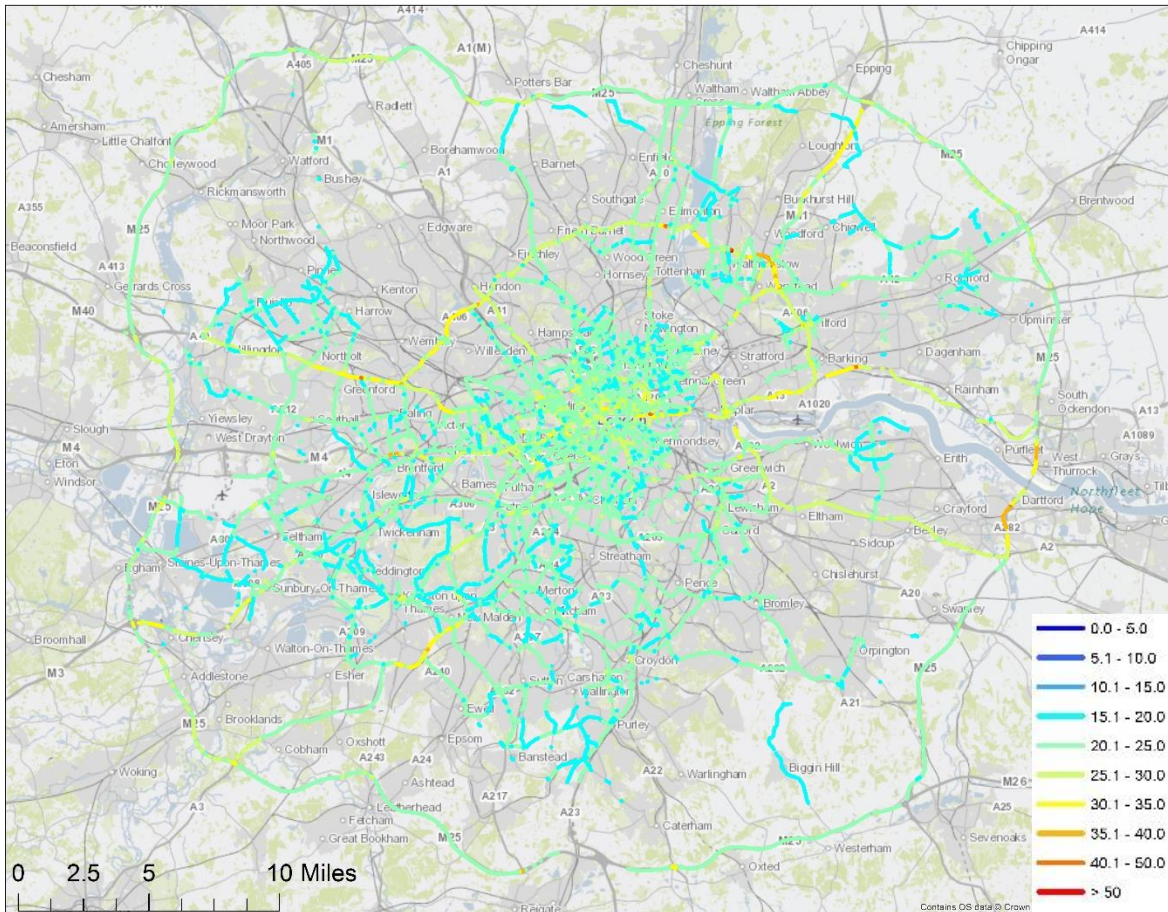


Figure 3-22 Period average modelled PM10 concentration ( $\mu\text{g}/\text{m}^3$ ) for each 30m driven road segment for the period 1 September 2018 to 31 October 2019.

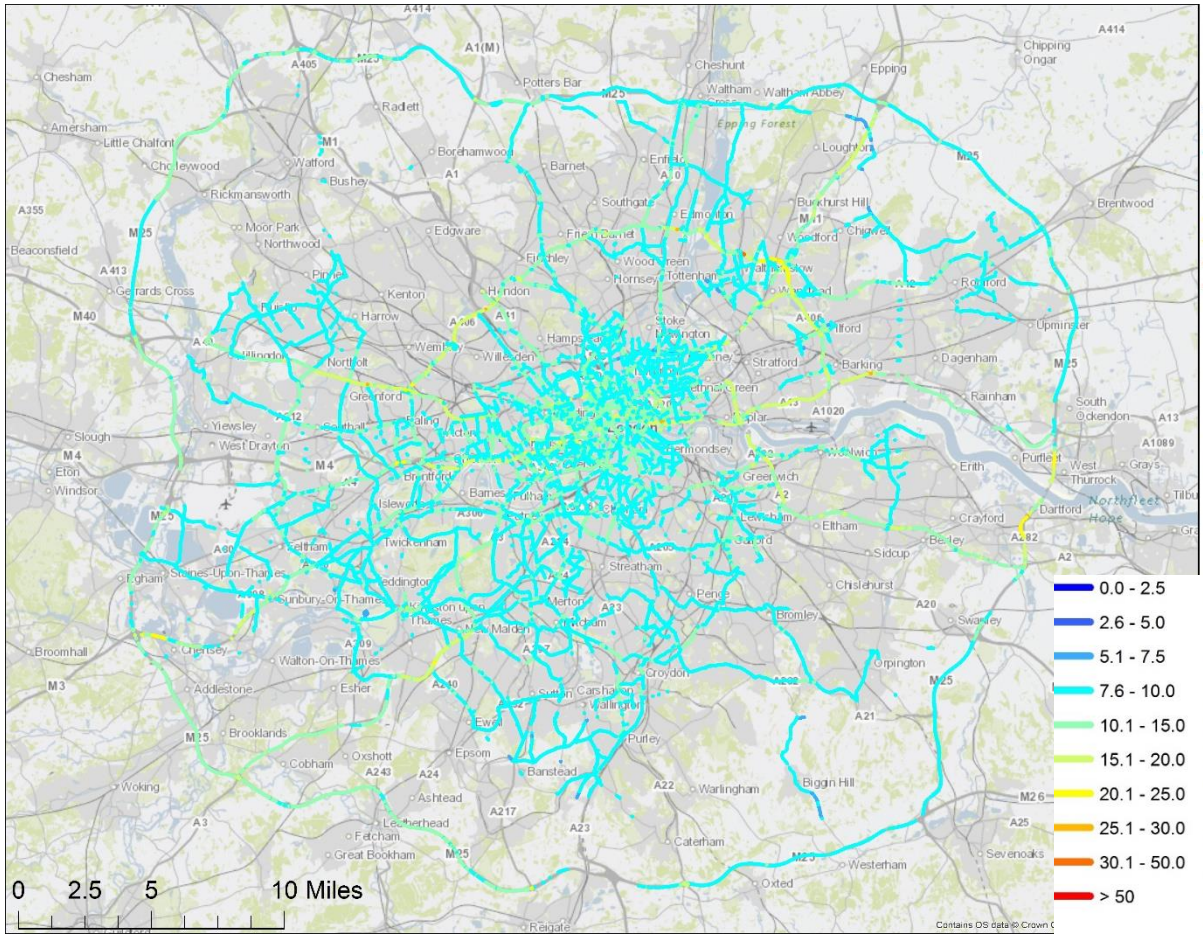


Figure 3-23 Period average modelled PM2.5 concentration (ug/m3) for each 30m driven road segment for the period 1 September 2018 to 31 October 2019.

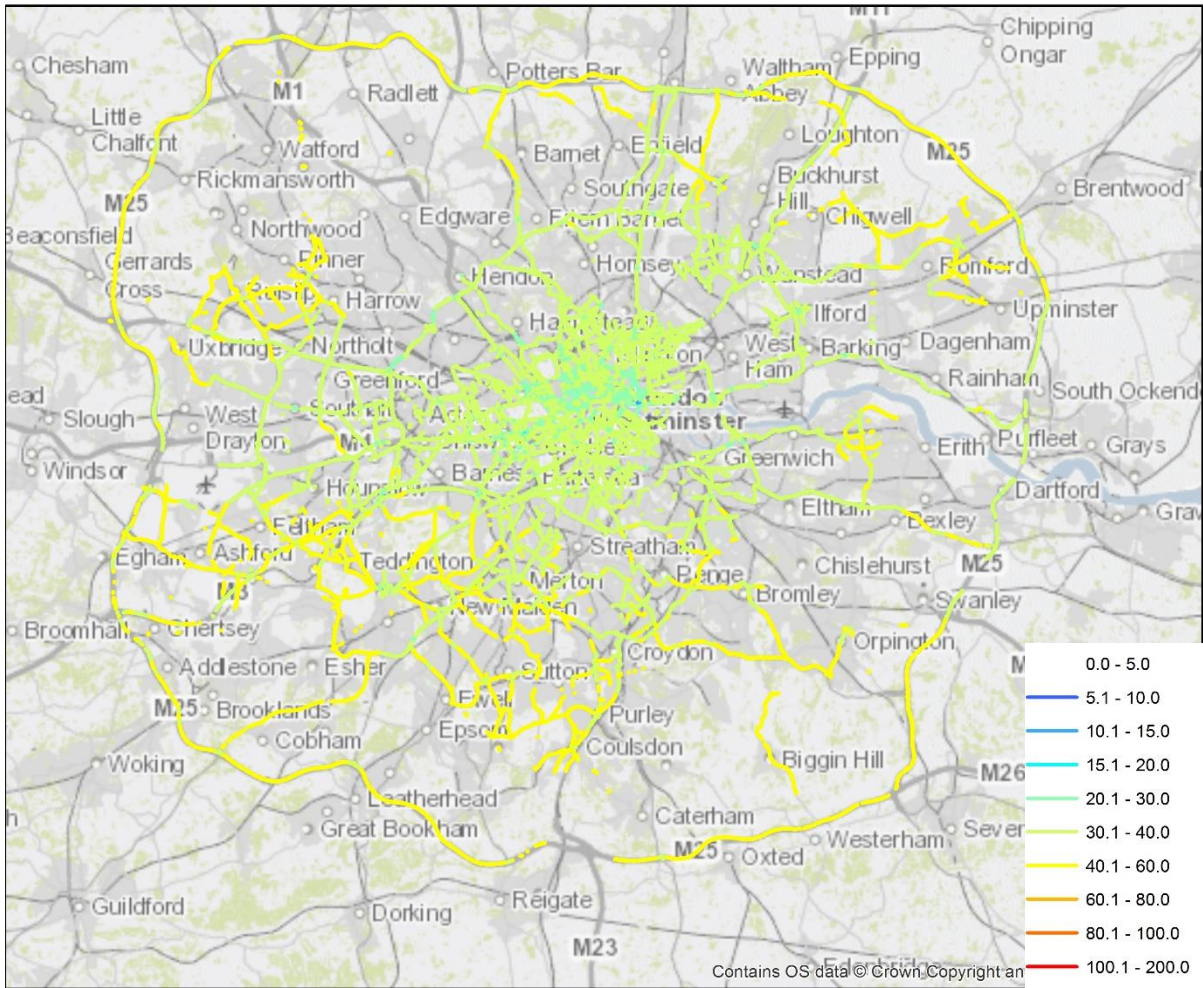


Figure 3-24 Period average modelled Ozone concentration (ug/m3) for each 30m driven road segment for the period 1 September 2018 to 31 October 2019.

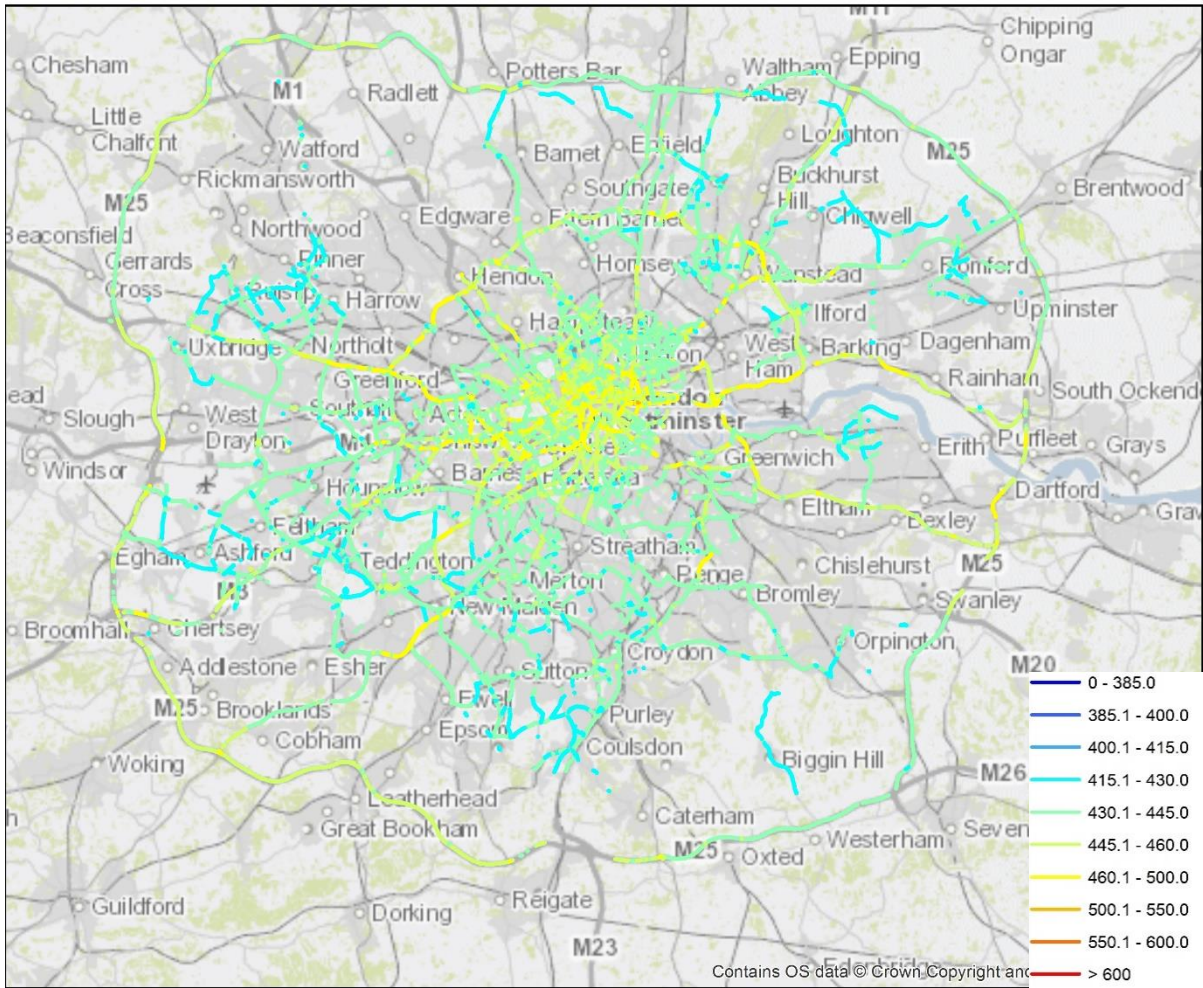


Figure 3-25 Period average modelled CO2 concentration (ppm) for each 30m driven road segment for the period 1 September 2018 to 31 October 2019.

## 4. Hotspot Analysis

### 4.1 Hangar Lane Gyratory, Ealing (EA6)

The modelled concentrations have large negative bias compared with measured values at EA6 for both NO<sub>2</sub> and PM<sub>10</sub> (Table 4-1, Figure 4-1). Investigation of this bias has shown that there is a sharp discontinuity in modelled concentrations as the North Circular enters the Hangar Lane Gyratory in the southbound direction (Figure 4-2). This appears to be caused by the LAEI having very low traffic flow on the North Circular as it passes round the Hanger Lane Gyratory and passes the EA6 monitor, compared with the section of the North Circular that feeds into the Hangar Lane Gyratory (Figure 4-3); the traffic flow on that section appears to be around 25% of the expected flow. The mobile measured concentrations (Figure 4-4) supports this conclusion.

Network	Number of Valid Values	Obs Mean $\mu\text{g}/\text{m}^3$	Mod Mean $\mu\text{g}/\text{m}^3$	MB $\mu\text{g}/\text{m}^3$	NMSE	R	FAC2
NO <sub>2</sub>	11540	64.2	37.5	-26.7	0.60	0.51	0.52
PM <sub>10</sub>	11684	24.7	13.8	-11.0	0.91	0.60	0.60

Table 4-1 Summary statistics for modelled and observed hourly mean NO<sub>2</sub> and PM<sub>10</sub> for LAQN site EA6. MB = Mean bias; NMSE = Normalised mean square error; R = correlation coefficient; FAC2 = percentage of modelled data points within a fraction of 2 of the measured value.

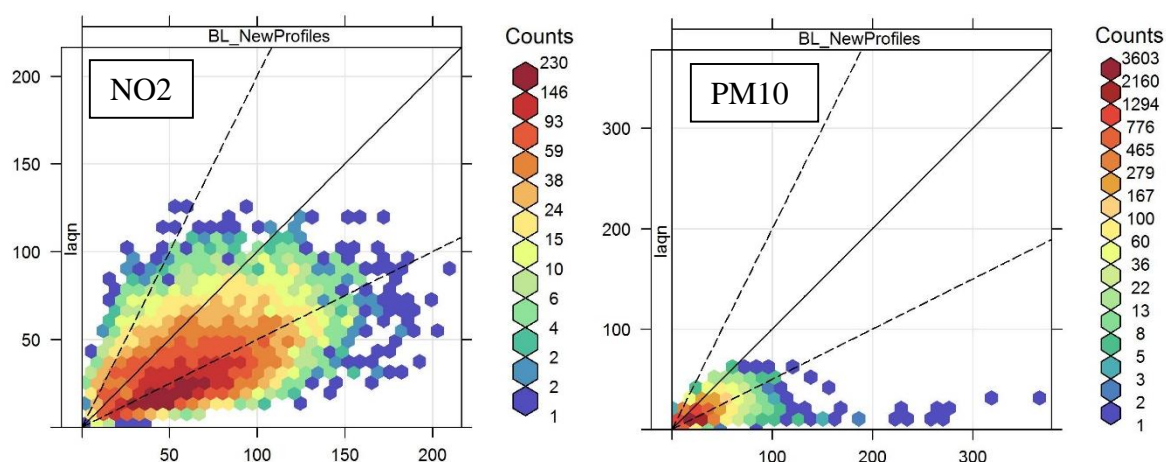


Figure 4-1 Modelled versus observed concentrations of NO<sub>2</sub> and PM<sub>10</sub> ( $\mu\text{g}/\text{m}^3$ ) at the EA6 LAQN site.

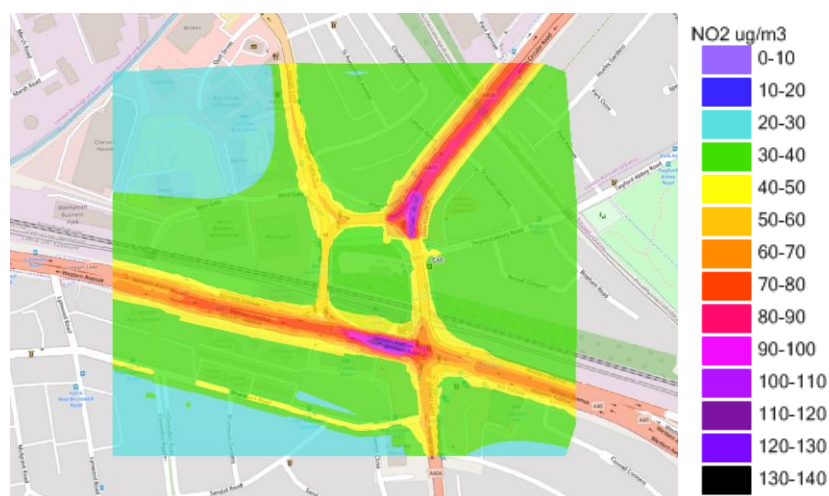


Figure 4-2 Average modelled NO<sub>2</sub> ( $\mu\text{g}/\text{m}^3$ ) around the Hangar Lane Gyratory. The EA6 monitor location is shown by the small green square.



Figure 4-3 Annual average daily traffic flows on the Hangar Lane Gyratory from the LAEI 2013, projection for 2020.

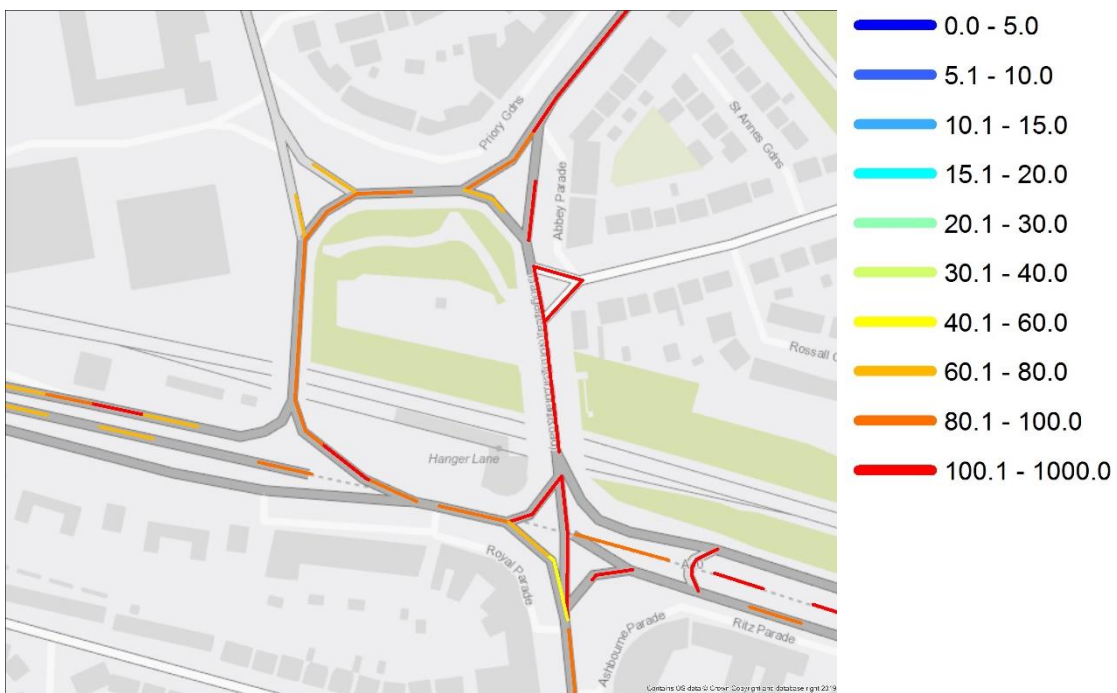


Figure 4-4 Average NO2 mobile Concentrations (ug/m3) on the Hangar Lane Gyratory over all driven hours

## 4.2 Holloway Bus Garage, Islington (54245)

The model displays a large negative bias at AQMesh site 54245 (Table 4-2, Figure 4-5). This is because the LAEI doesn't include the bus garage, either in the road traffic information or the gridded emissions. To model it accurately we would need to have detailed information about bus movements in and out of the garage in order to characterise the source.

Network	Number of Valid Values	Obs Mean $\mu\text{g}/\text{m}^3$	Mod Mean $\mu\text{g}/\text{m}^3$	MB $\mu\text{g}/\text{m}^3$	NMSE	R	FAC2
NO2	11867	61.3	29.1	-32.2	1.73	0.00	0.50
PM2.5	11886	13.0	7.0	-6.0	0.88	0.86	0.57

Table 4-2 Summary statistics for modelled and observed hourly mean NO<sub>2</sub> and PM<sub>2.5</sub> for AQMesh site 54245. MB = Mean bias; NMSE = Normalised mean square error; R = correlation coefficient; FAC2 = percentage of modelled data points within a fraction of 2 of the measured value.

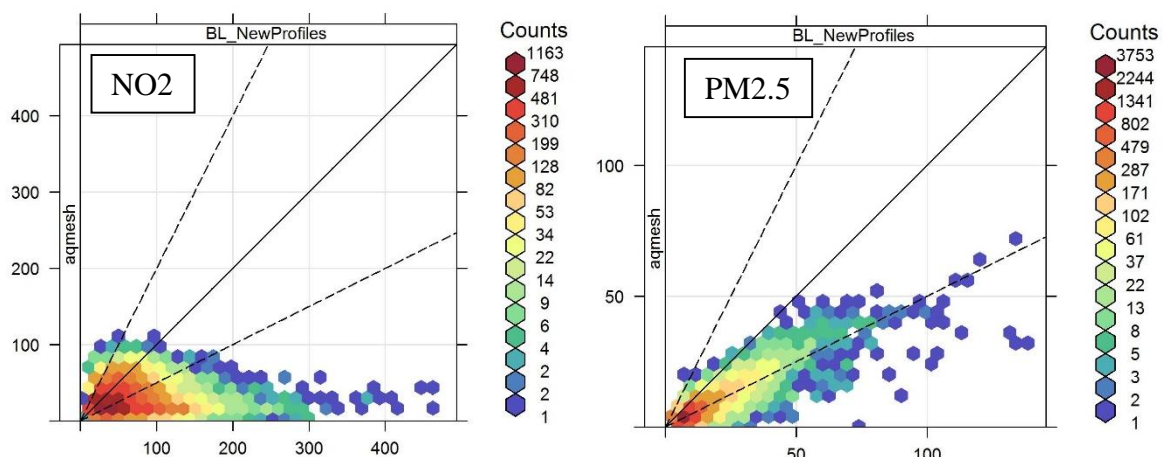


Figure 4-5 Modelled versus observed concentrations of NO<sub>2</sub> and PM<sub>2.5</sub> ( $\mu\text{g}/\text{m}^3$ ) at the 54245 AQMesh site.



Figure 4-6 Average modelled NO<sub>2</sub> ( $\mu\text{g}/\text{m}^3$ ) around the Holloway Bus Garage. The AQMesh monitor locations are shown by the small green squares.

### 4.3 Lambeth – Brixton Road (LB4)

The model displays a large negative bias at LAQN site LB4 (Table 4-3, Figure 4-7). This is because the monitor is in a deep street canyon, and the receptor location has placed it outside the modelled street canyon. Moving the receptor a short distance (~2m) will place it inside the canyon and accurately represent the location of the site with respect to the road topography increasing concentrations – see contour plot (Figure 4-8).

Network	Number of Valid Values	Obs Mean $\mu\text{g}/\text{m}^3$	Mod Mean $\mu\text{g}/\text{m}^3$	MB $\mu\text{g}/\text{m}^3$	NMSE	R	FAC2
NO2	8233	73.4	31.1	-42.3	1.11	0.57	0.35
PM10	8054	25.3	12.7	-12.6	0.70	0.82	0.45

Table 4-3 Summary statistics for modelled and observed hourly mean NO<sub>2</sub> and PM<sub>10</sub> for LAQN site LB4. MB = Mean bias; NMSE = Normalised mean square error; R = correlation coefficient; FAC2 = percentage of modelled data points within a fraction of 2 of the measured value.

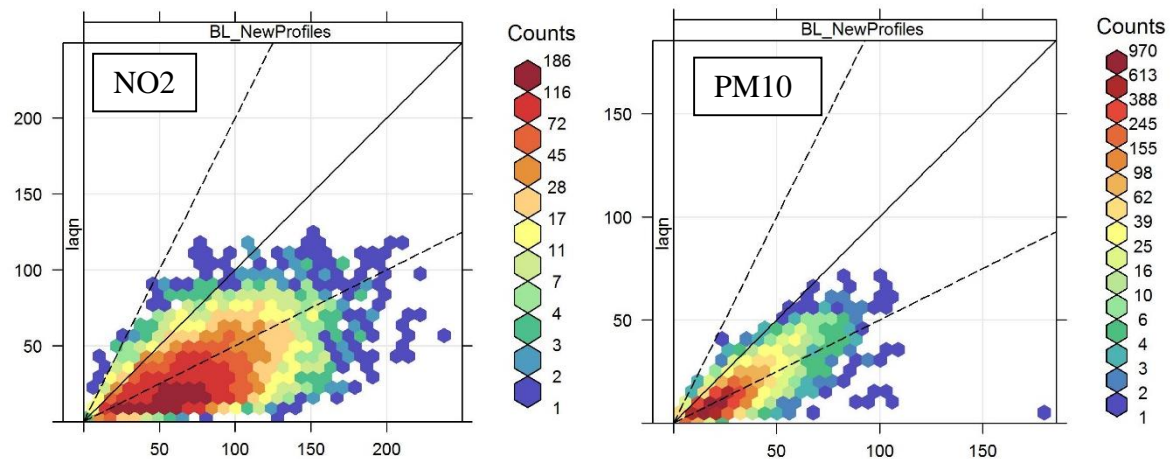


Figure 4-7 Modelled versus observed concentrations of NO<sub>2</sub> and PM<sub>10</sub> ( $\mu\text{g}/\text{m}^3$ ) at the LB4 LAQN site.

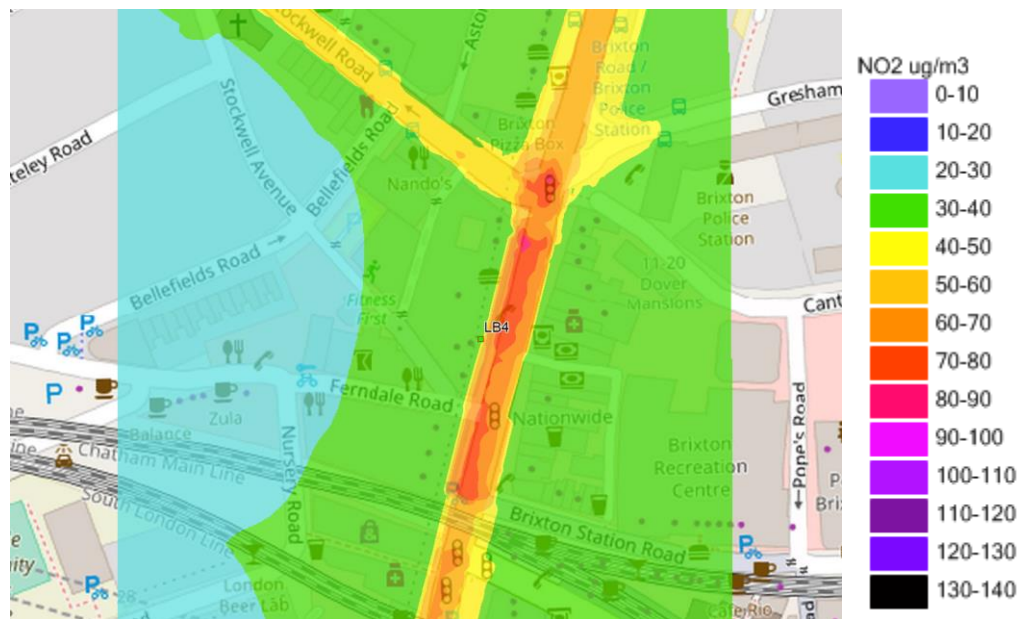


Figure 4-8 Average modelled NO<sub>2</sub> ( $\mu\text{g}/\text{m}^3$ ) around the LB4 site. The monitor location is shown by the small green square.

## 4.4 Croydon – Purley Way A23 (CR7)

The model has a significant positive bias here (Table 4-4, Figure 4-9). The monitor is located within the school grounds and is behind a fence that surrounds it. Also the model has a high canyon on the monitor side of the road, but the monitor is actually in a gap. To reduce the model bias the road source needs to be divided into two parts and the canyon geometry made more precise near the monitor. In addition the model receptor needs to be moved further from the edge of the road.

Network	Number of Valid Values	Obs Mean $\mu\text{g}/\text{m}^3$	Mod Mean $\mu\text{g}/\text{m}^3$	MB $\mu\text{g}/\text{m}^3$	NMSE	R	FAC2
<b>NO2</b>	12256	28.5	37.1	8.55	0.42	0.65	0.78

Table 4-4 Summary statistics for modelled and observed hourly mean  $\text{NO}_2$  and  $\text{PM}_{10}$  for LAQN site LB4. MB = Mean bias; NMSE = Normalised mean square error; R = correlation coefficient; FAC2 = percentage of modelled data points within a fraction of 2 of the measured value.

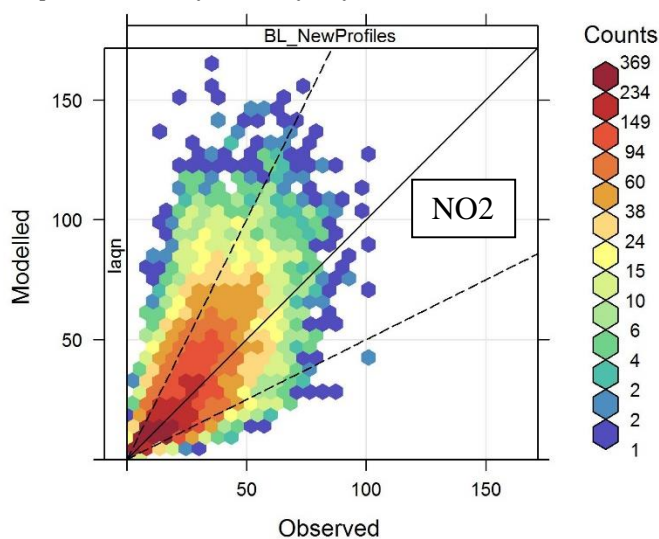


Figure 4-9 Modelled versus observed concentrations of  $\text{NO}_2$  ( $\mu\text{g}/\text{m}^3$ ) at the CR7 LAQN site.

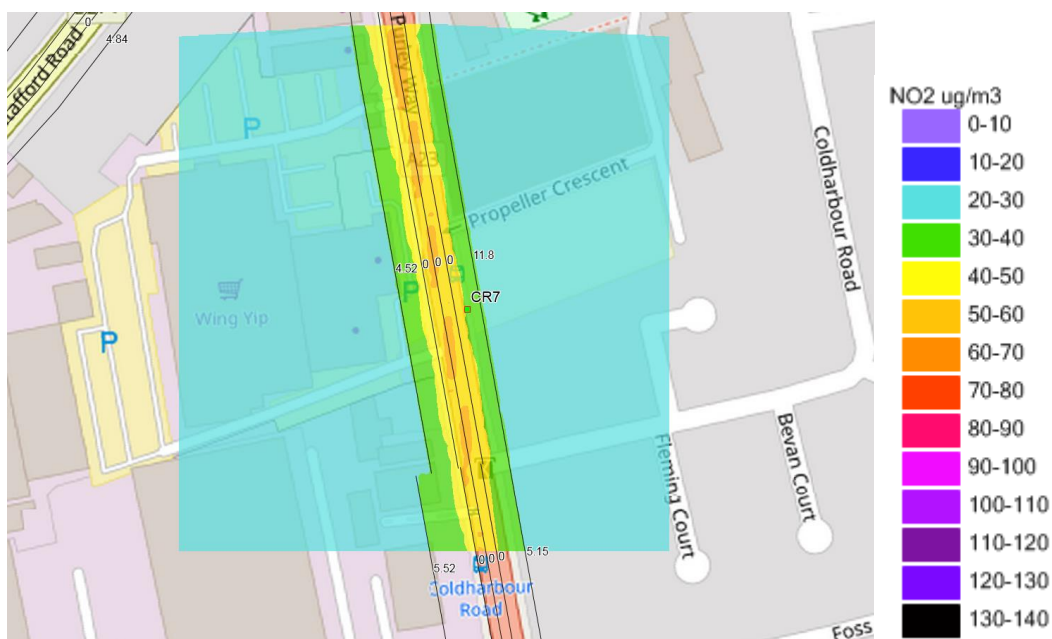


Figure 4-10 Average modelled  $\text{NO}_2$  ( $\mu\text{g}/\text{m}^3$ ) around the CR7 site. The monitor location is shown by the small green square.

## 4.5 City of London – Beech Street (CT4)

The model has a significant bias here. This is a highly complex site: Beech Street is in a tunnel underneath the Barbican Centre, so the monitor is in the tunnel. CERC has modelled this in detail for City of London in the past and a similarly detailed approach would be necessary to improve the agreement here.

Network	Number of Valid Values	Obs Mean $\mu\text{g}/\text{m}^3$	Mod Mean $\mu\text{g}/\text{m}^3$	MB $\mu\text{g}/\text{m}^3$	NMSE	R	FAC2
NO <sub>2</sub>	12144	60.0	40.8	-19.2	0.39	0.57	0.72
PM <sub>10</sub>	11888	21.7	14.5	-7.3	0.42	0.78	0.78

Table 4-5 Summary statistics for modelled and observed hourly mean NO<sub>2</sub> and PM<sub>10</sub> for LAQN site CT4. MB = Mean bias; NMSE = Normalised mean square error; R = correlation coefficient; FAC2 = percentage of modelled data points within a fraction of 2 of the measured value.

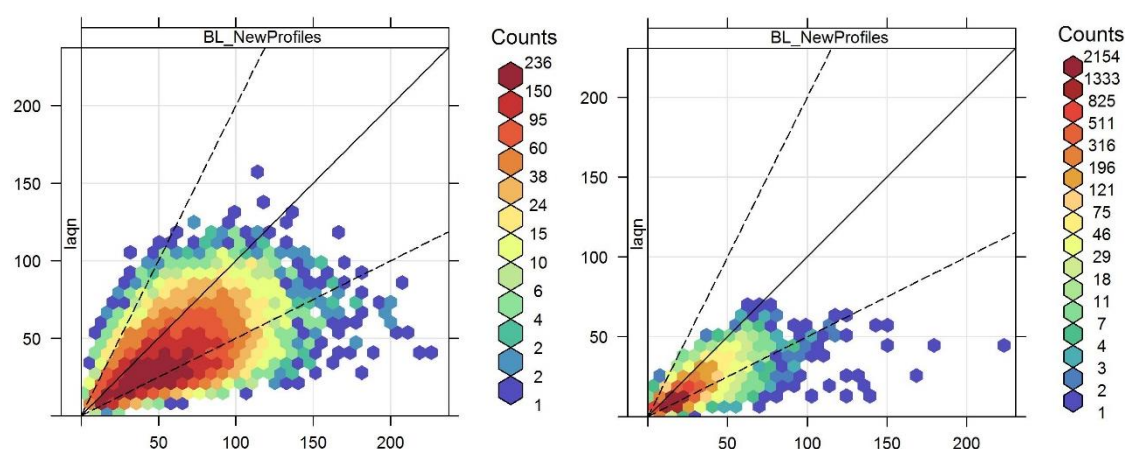


Figure 4-11 Modelled versus observed concentrations of NO<sub>2</sub> and PM<sub>10</sub> ( $\mu\text{g}/\text{m}^3$ ) at the CT4 LAQN site.

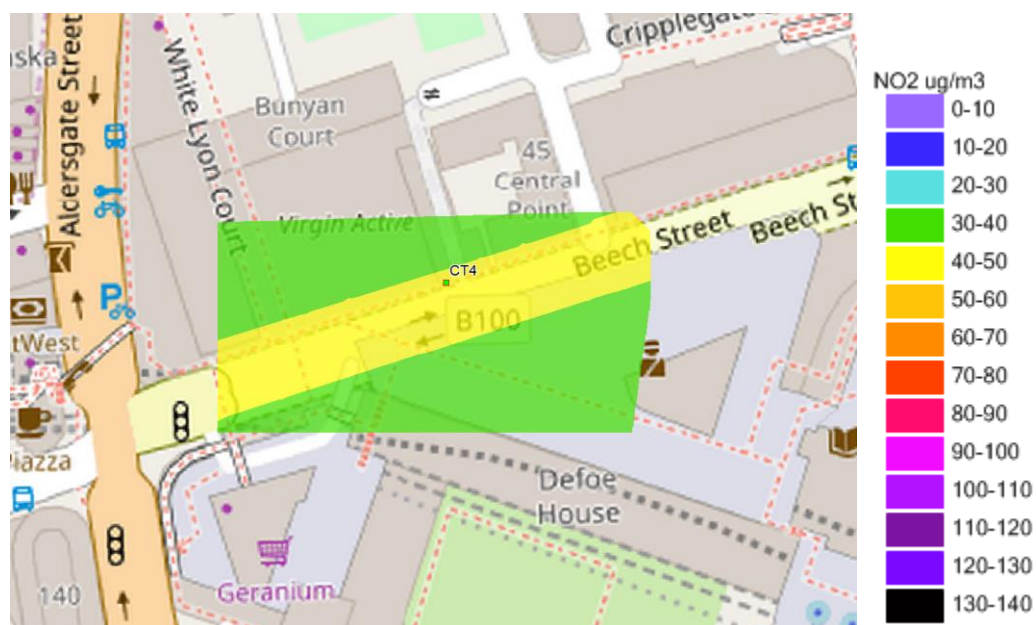


Figure 4-12 Average modelled NO<sub>2</sub> ( $\mu\text{g}/\text{m}^3$ ) around the CT4 site. The monitor location is shown by the small green square.

## 4.6 Westminster – Strand (Northbank BID) (NB1)

The model has a negative bias here. The LAEI AADTs on the Strand look too low, because the flow coming in from the east and the flow going round the gyratory are much more than the flow on the Strand, and the flow is one way. Mobile measurements support this (Figure 4-16).

Network	Number of Valid Values	Obs Mean $\mu\text{g}/\text{m}^3$	Mod Mean $\mu\text{g}/\text{m}^3$	MB $\mu\text{g}/\text{m}^3$	NMSE	R	FAC2
<b>NO2</b>	12048	75.1	53.2	-21.9	0.30	0.56	0.76

Table 4-6 Summary statistics for modelled and observed hourly mean  $\text{NO}_2$  for LAQN site NB1. MB = Mean bias; NMSE = Normalised mean square error; R = correlation coefficient; FAC2 = percentage of modelled data points within a fraction of 2 of the measured value.

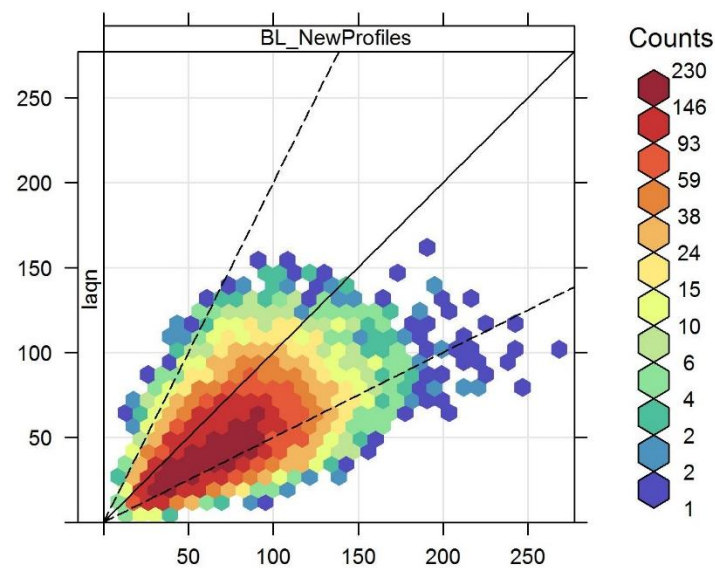


Figure 4-13 Modelled versus observed concentrations of  $\text{NO}_2$  ( $\mu\text{g}/\text{m}^3$ ) at the NB1 LAQN site.

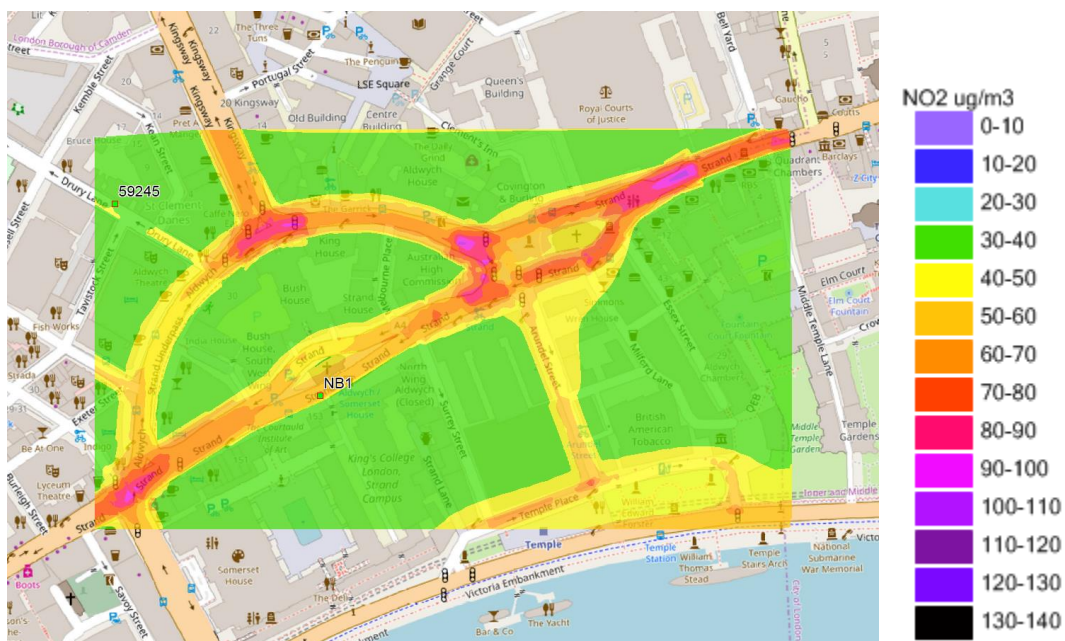


Figure 4-14 Average modelled  $\text{NO}_2$  ( $\mu\text{g}/\text{m}^3$ ) around the NB1 site. The monitor location is shown by the small green square.

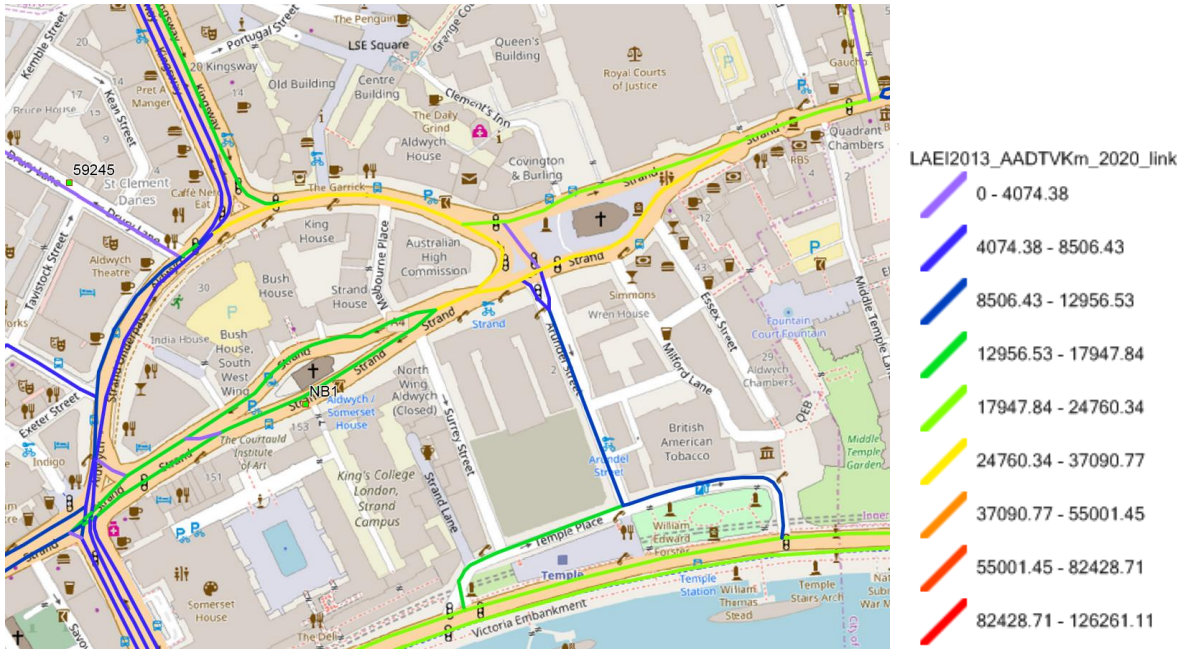


Figure 4-15 Annual average daily traffic flows near the NBI monitor from the LAEI 2013, projection for 2020.

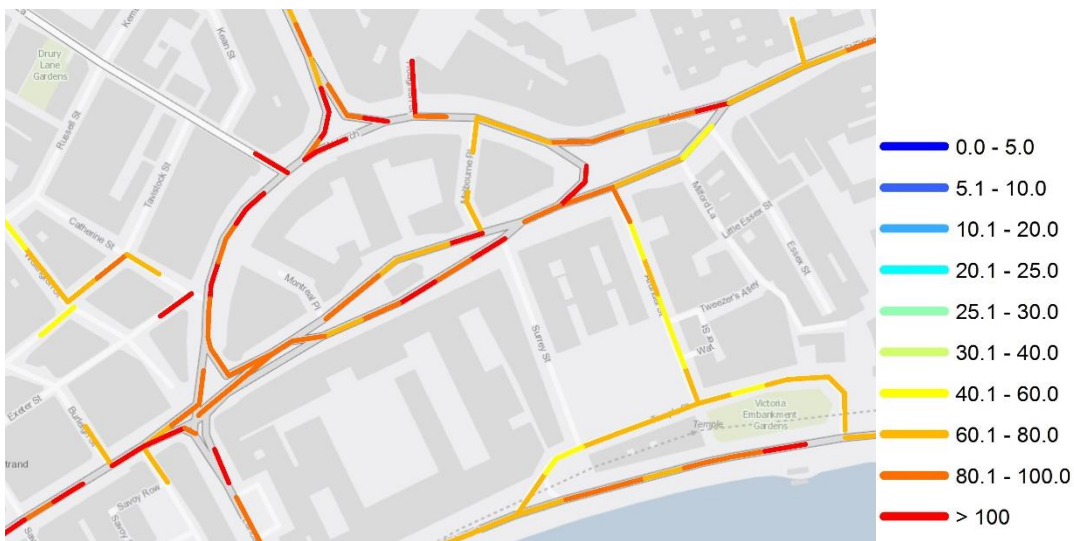


Figure 4-16 Average observed NO<sub>2</sub> (ug/m<sup>3</sup>) mobile averages around the NBI site.

## 4.7 Kingston – London Road (18245)

The model has a significant negative bias here (Table 4-7, Figure 4-16). The site is on a busy junction; however, the concentration contours (Figure 4-17) show a drop in concentrations in the immediate vicinity of the monitor. Traffic flows on the roads immediately adjacent to the site are zero in the LAEI (Figure 4-18), which is likely to be the cause of the model underestimate. The mobile data (Figure 4-19) supports this argument, because measured concentrations on this junction are as high as on the surrounding roads.

Network	Number of Valid Values	Obs Mean $\mu\text{g}/\text{m}^3$	Mod Mean $\mu\text{g}/\text{m}^3$	MB $\mu\text{g}/\text{m}^3$	NMSE	R	FAC2
<b>NO2</b>	6809	46.7	31.1	-15.6	0.47	0.55	0.60
<b>PM2.5</b>	8538	9.3	7.1	-2.2	0.48	0.86	0.78

Table 4-7 Summary statistics for modelled and observed hourly mean NO<sub>2</sub> and PM<sub>10</sub> for AQMesh site 18245. MB = Mean bias; NMSE = Normalised mean square error; R = correlation coefficient; FAC2 = percentage of modelled data points within a fraction of 2 of the measured value.

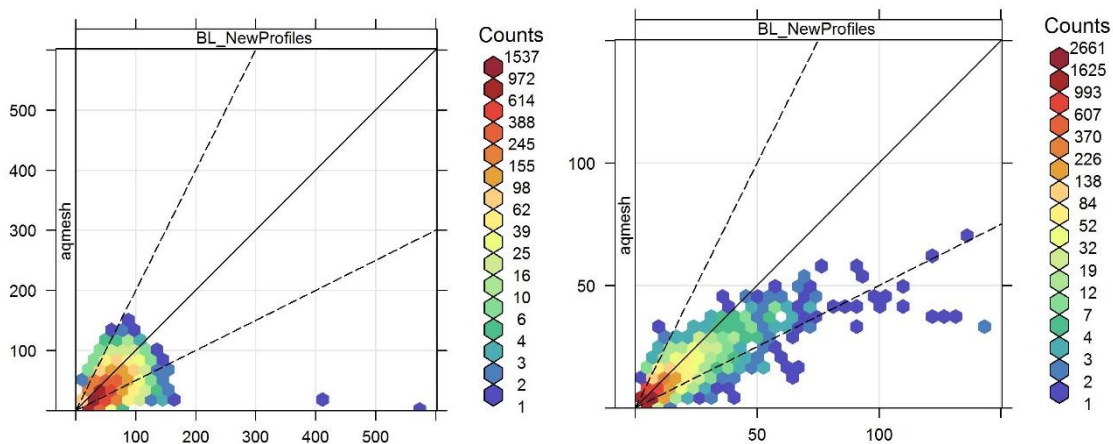


Figure 4-16 Modelled versus observed concentrations of NO<sub>2</sub> and PM<sub>10</sub> ( $\mu\text{g}/\text{m}^3$ ) at the 18245 AQMesh site.

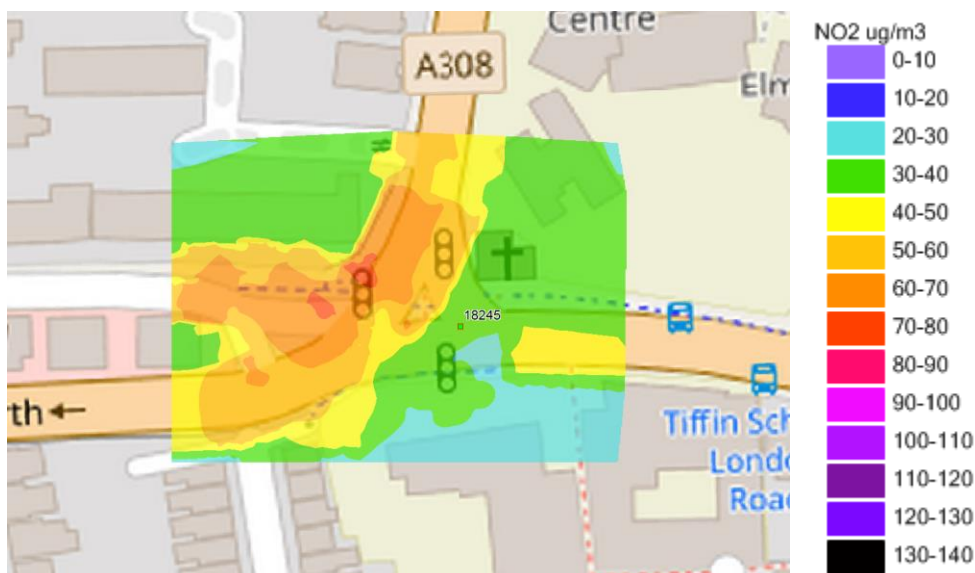


Figure 4-17 Average modelled NO<sub>2</sub> ( $\mu\text{g}/\text{m}^3$ ) around the 18245 site. The monitor location is shown by the small green square.



Figure 4-18 Annual average daily traffic flows (AADT) near the 18245 monitor from the LAEI 2013, projection for 2020.



Figure 4-19 Average observed NO2 (ug/m3) mobile averages around the 18245 site

## 4.8 Barking and Dagenham – Station Parade (37245)

The model has a large negative bias at this site (Table 4-8, Figure 4-20). The site is outside Barking Station where there are many bus stops, but the contour plot shows no elevated concentrations in this area (Figure 4-21). However, the LAEI has no road data all around the station (Figure 4-22), which is likely to be the case of the model underestimation.

Network	Number of Valid Values	Obs Mean $\mu\text{g}/\text{m}^3$	Mod Mean $\mu\text{g}/\text{m}^3$	MB $\mu\text{g}/\text{m}^3$	NMSE	R	FAC2
NO2	12006	56.7	30.4	-26.3	0.62	0.58	0.48
PM2.5	12015	13.5	7.5	-6.0	0.69	0.81	0.56

Table 4-8 Summary statistics for modelled and observed hourly mean NO<sub>2</sub> and PM<sub>2.5</sub> for AQMesh site 37245. MB = Mean bias; NMSE = Normalised mean square error; R = correlation coefficient; FAC2 = percentage of modelled data points within a fraction of 2 of the measured value.

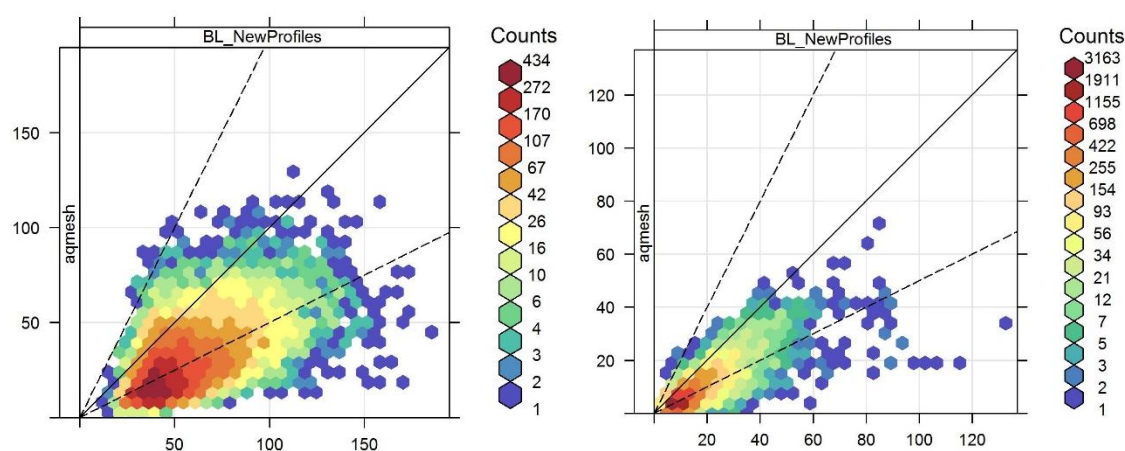


Figure 4-20 Modelled versus observed concentrations of NO<sub>2</sub> and PM<sub>2.5</sub> ( $\mu\text{g}/\text{m}^3$ ) at the 37245 AQMesh site.



Figure 4-21 Average modelled NO<sub>2</sub> ( $\mu\text{g}/\text{m}^3$ ) around the 37245 site. The monitor location is shown by the small green square.

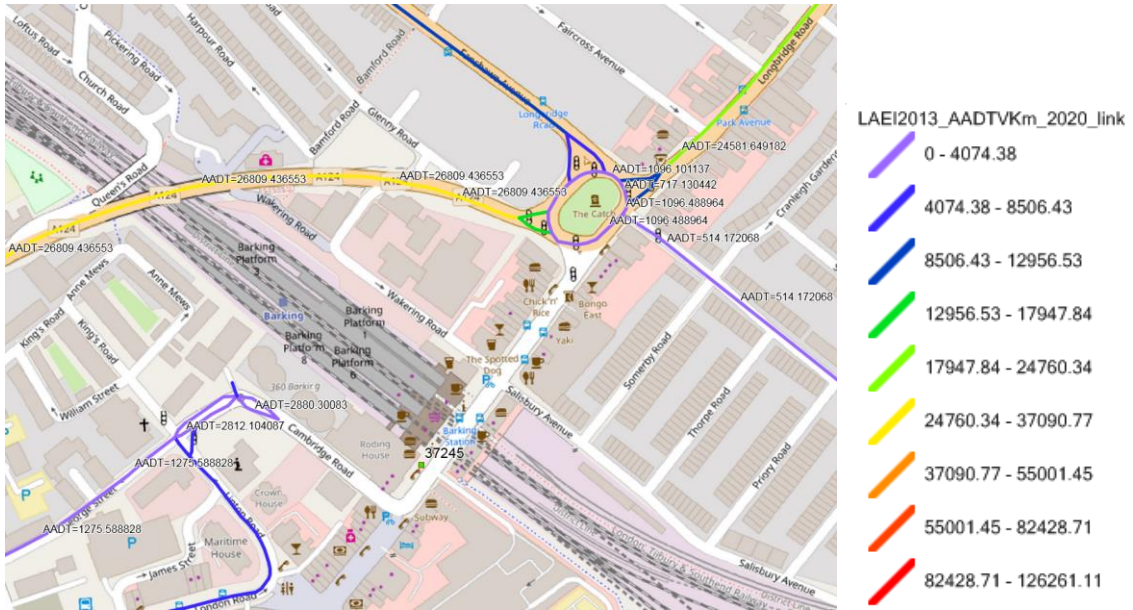


Figure 4-22 Annual average daily traffic flows (AADT) near the 37245 monitor from the LAEI 2013, projection for 2020.

## 4.9 Hackney – Cecilia Road (78245)

The model has a large negative bias at this site (Table 4-9, Figure 4-23). The NO<sub>2</sub> contour plot (Figure 4-24) shows generally low levels in this area, with little spatial variation. The LAEI includes traffic flows for Cecilia Road but is missing Sandringham Road, one of the roads on the crossroads where the monitor is located (Figure 4-25). In this case, the model underestimate may be partly caused by Sandringham being missing, but traffic flows in this area are generally relatively low, so including this missing road is unlikely to increase modelled concentrations at 78245 substantially. The AQMesh monitor is not reading any concentrations below around 20  $\mu\text{g}/\text{m}^3$ , which could be due to ozone cross-interference, temperature sensitivity or long-term upwards drift, and this may be the dominant cause of the bias in this case.

Network	Number of Valid Values	Obs Mean $\mu\text{g}/\text{m}^3$	Mod Mean $\mu\text{g}/\text{m}^3$	MB $\mu\text{g}/\text{m}^3$	NMSE	R	FAC2
NO <sub>2</sub>	9194	46.4	29.9	-16.5	0.38	0.53	0.62
PM <sub>2.5</sub>	7626	8.4	6.1	-2.3	0.33	0.79	0.73

Table 4-9 Summary statistics for modelled and observed hourly mean NO<sub>2</sub> and PM<sub>2.5</sub> for AQMesh site 78245. MB = Mean bias; NMSE = Normalised mean square error; R = correlation coefficient; FAC2 = percentage of modelled data points within a fraction of 2 of the measured value.

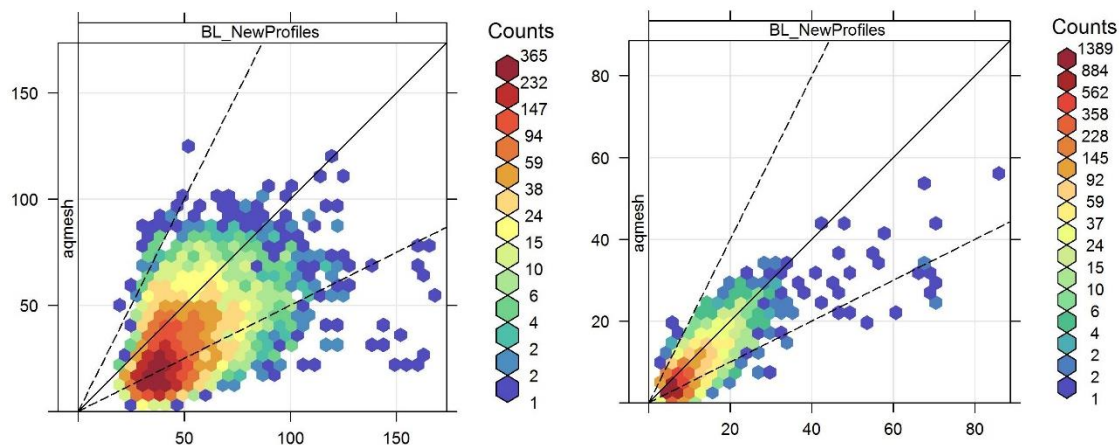


Figure 4-23 Modelled versus observed concentrations of NO<sub>2</sub> and PM<sub>2.5</sub> ( $\mu\text{g}/\text{m}^3$ ) at the 78245 AQMesh site.

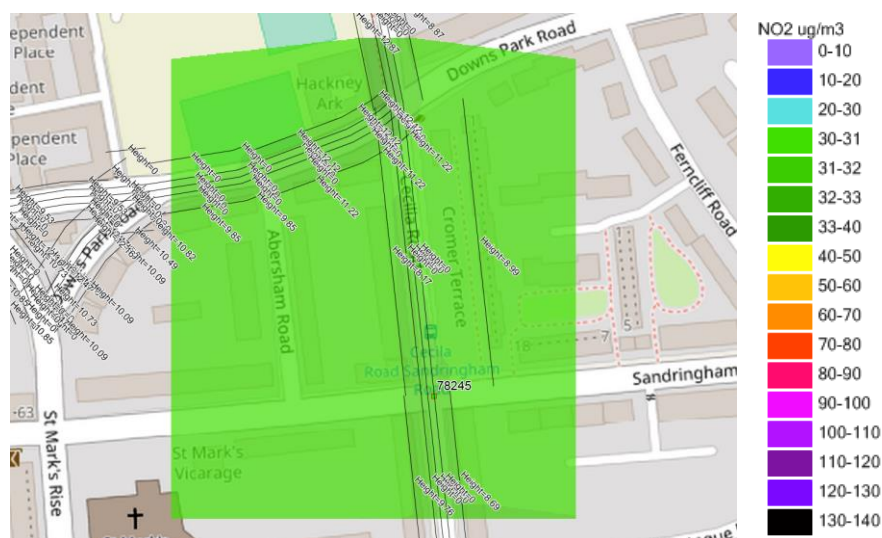


Figure 4-24 Average modelled NO<sub>2</sub> ( $\mu\text{g}/\text{m}^3$ ) around the 78245 site. The monitor location is shown by the small green square. Modelled road topography heights are labelled.

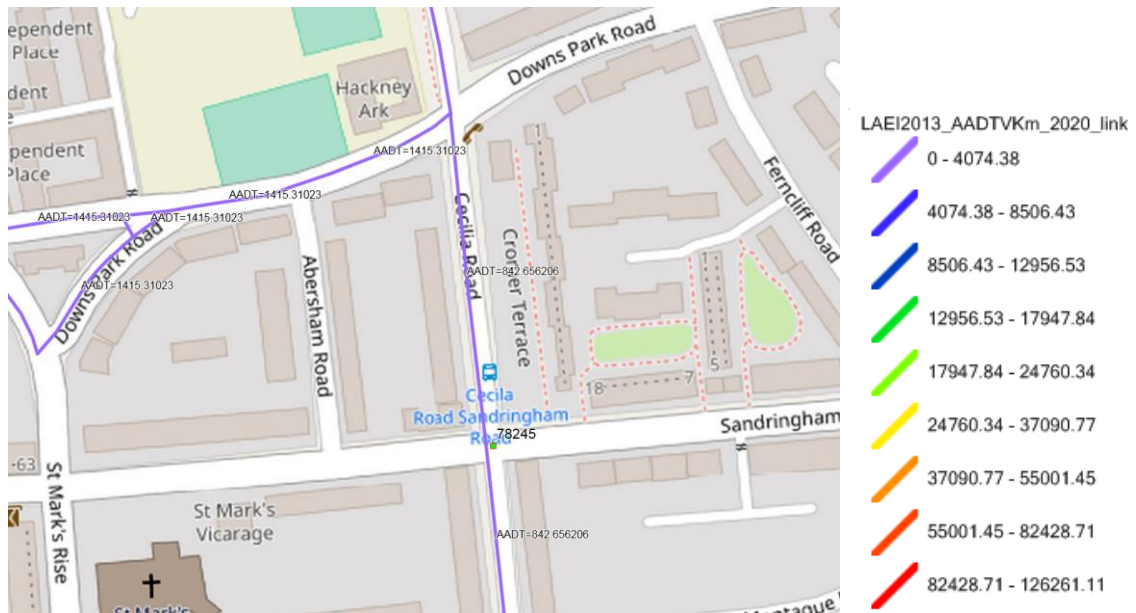


Figure 4-25 Annual average daily traffic flows (AADT) near the 78245 monitor from the LAEI 2013, projection for 2020.

## 4.10 Hillingdon – Ruislip High Street (92245)

The model has a large negative bias at this site (Table 4-10, Figure 4-26). The contour plot of average NO<sub>2</sub> concentrations (Figure 4-27) shows that the roads near the site are modelled, and the receptor location and road topography are reasonable. This monitor is located towards the top of a lamppost at around 7m. The LAEI traffic flows look reasonable in this area (Figure 4-28), however traffic speeds on the road segment passing the monitor and approaching the junction seem too high, and this could be contributing to the model underestimation. The bus stop near to the site may also be a factor. As with 78245, the AQMesh monitor here is reading few concentrations below around 20 ug/m<sup>3</sup>, which could be due to ozone cross-interference, temperature sensitivity or long-term upwards drift, and this may be the dominant cause of the bias in this case.

Network	Number of Valid Values	Obs Mean $\mu\text{g}/\text{m}^3$	Mod Mean $\mu\text{g}/\text{m}^3$	MB $\mu\text{g}/\text{m}^3$	NMSE	R	FAC2
NO <sub>2</sub>	9263	48.5	26.6	-21.9	0.57	0.65	0.46

Table 4-10 Summary statistics for modelled and observed hourly mean NO<sub>2</sub> for AQMesh site 92245. MB = Mean bias; NMSE = Normalised mean square error; R = correlation coefficient; FAC2 = percentage of modelled data points within a fraction of 2 of the measured value.

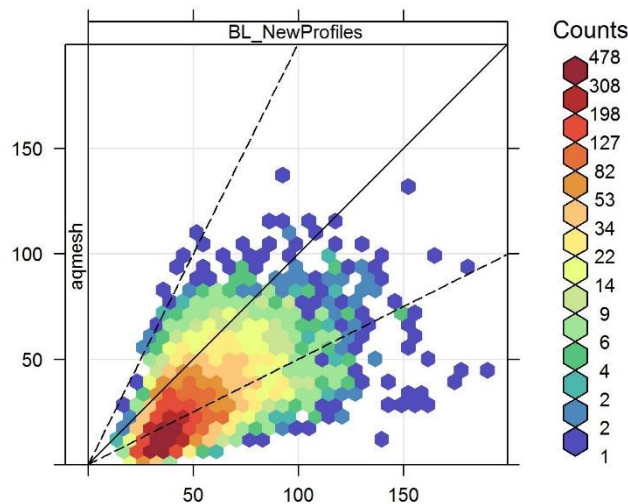


Figure 4-26 Modelled versus observed concentrations of NO<sub>2</sub> (ug/m<sup>3</sup>) at the 92245 AQMesh site.



Figure 4-27 Average modelled NO<sub>2</sub> (ug/m<sup>3</sup>) around the 92245 site. The monitor location is shown by the small green square. Modelled road topography heights are labelled.

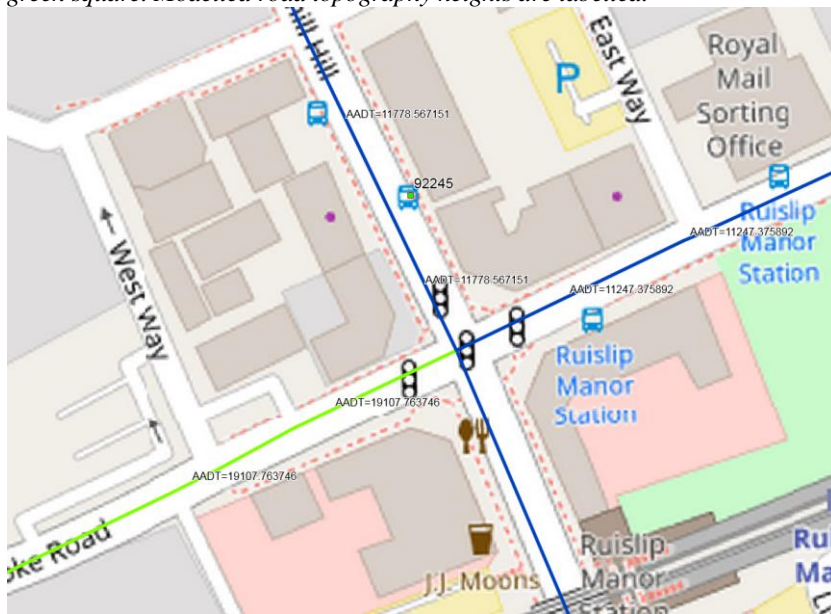


Figure 4-28 Annual average daily traffic flows (AADT) near the 92245 monitor from the LAEI 2013, projection for 2020.

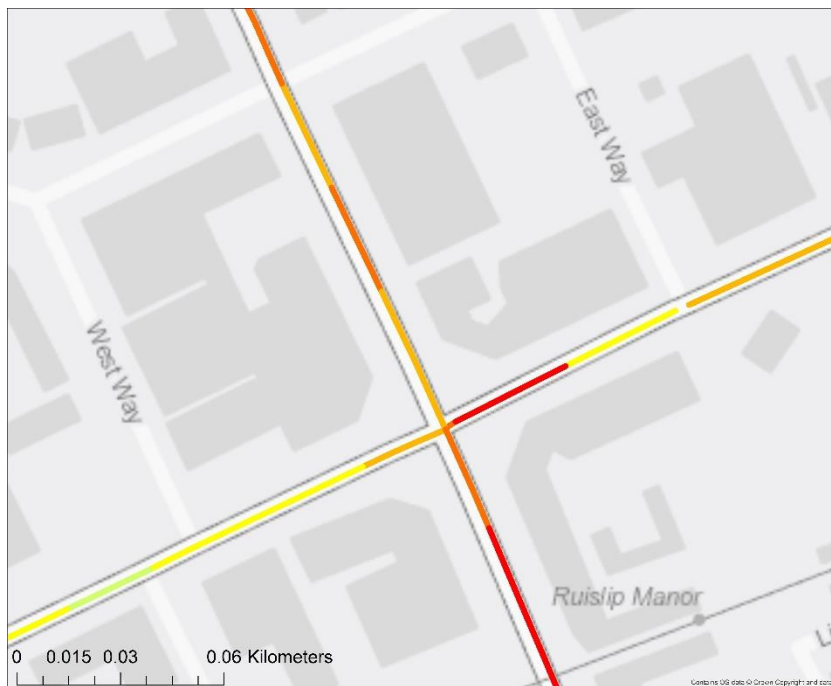


Figure 4-29 Average observed NO<sub>2</sub> (ug/m<sup>3</sup>) mobile averages around the 92245 site.

## 4.11 Southwark – New Kent Road

This hotspot was identified from the bias between the modelled and mobile data – concentrations are significantly higher in the mobile measured data. This is likely to be due to more congestion and slower speeds in reality than in the LAEI.



Figure 4-30 Average mobile measured (left) and modelled (right) NO<sub>2</sub> concentrations ( $\mu\text{g}/\text{m}^3$ ) around the Elephant and Castle roundabout and New Kent Road.



Figure 4-31 Average modelled NO<sub>2</sub> concentrations ( $\mu\text{g}/\text{m}^3$ ) around the Elephant and Castle roundabout and New Kent Road.

## 4.12 Embankment

This is another hotspot identified from the comparison of mobile and measured data. Concentrations on Embankment are significantly higher in the measured concentrations than in the modelled results. This is likely to be due to more congestion than is represented in the LAEI.

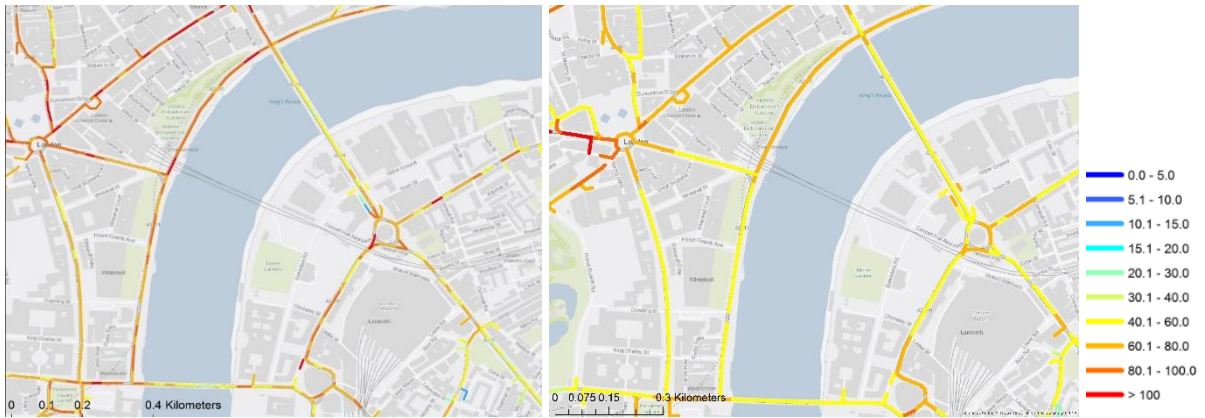


Figure 4-32 Average mobile measured (left) and modelled (right) NO<sub>2</sub> concentrations ( $\mu\text{g}/\text{m}^3$ ) in the Embankment area.

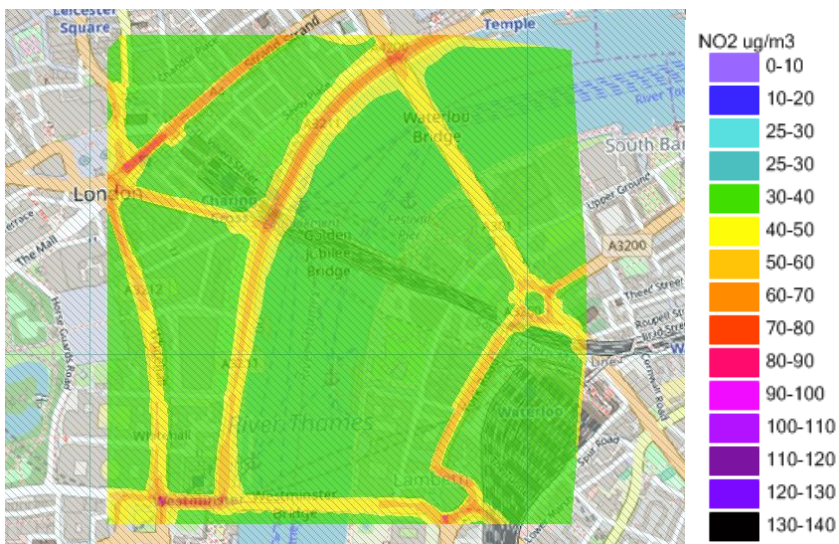


Figure 4-33 Average modelled NO<sub>2</sub> concentrations ( $\mu\text{g}/\text{m}^3$ ) around Embankment.

## **5. Discussion and Recommendations**

### **5.1 LAEI issues**

The analysis in this report has shown that there are some areas where the LAEI appears to significantly underestimate traffic flows, such as the Hangar Lane Gyratory in Ealing, the Strand in Westminster, the London Road junction in Kingston and around Barking Station. While some of these can be addressed for the next round of modelling (Hangar Lane Gyratory, Strand, London Road junction), others such as the lack of any road flows near Barking Station need further information and cannot be improved within the scope of this project. We would recommend that these areas are given attention in future versions of the LAEI.

### **5.2 Time-varying emissions profiles**

The analysis in this report has identified that the diurnal profiles used for the modelling need some further work, to deal with the one-hour offset, to correct the overestimates on Sunday evenings and to represent the variation in traffic flows across the week from Monday to Sunday.

### **5.3 Monitor location adjustments**

Some minor adjustments to monitor locations will improve the representation of the monitoring sites in the modelling, for example LB4 needs to be moved from outside to inside the street canyon to correct the negative bias; CR7 is currently overestimated and this could be improved by better representation of the street canyon detail in this area.

### **5.4 Queuing**

Some model underestimates could be attributed to more congestion than is represented in the LAEI. This applies to Ruislip High Street in Hillingdon (92245), the Embankment and the Elephant and Castle roundabout and approach.

### **5.5 Remaining issues**

Some differences between modelled and measured concentrations would require further work outside the scope of this project to address fully. The Holloway bus garage is not represented in the LAEI and to characterise the emissions from this source would require detailed information about bus movements in and out of the garage. CT4 at Beech Street is in a highly complex environment, which has been modelled using ADMS-Urban in the past but would require significant further work to integrate with the Breathe London modelling. Barking station has no road traffic flows in the LAEI so the model will continue to underestimate concentrations at station 37245.

## APPENDIX A: Summary of ADMS-Urban

ADMS-Urban is a scientifically advanced but practical air pollution modelling tool, which has been developed to provide high resolution calculations of pollution concentrations for all sizes of study area relevant to the urban environment. The model can be used to look at concentrations near a single road junction or over a region extending across the whole of a major city. ADMS-Urban has been extensively used for the Review and Assessment of Air Quality carried out by Local Authorities in the UK and for a wide range of planning and policy studies across the world. The following is a summary of the capabilities and validation of ADMS-Urban. More details can be found on the CERC web site at [www.cerc.co.uk](http://www.cerc.co.uk).

ADMS-Urban is a development of the Atmospheric Dispersion Modelling System (ADMS), which has been developed to investigate the impacts of emissions from industrial facilities. ADMS-Urban allows full characterisation of the wide variety of emissions in urban areas, including an extensively validated road traffic emissions model. It also includes a number of other features, which include consideration of:

- the effects of vehicle movement on the dispersion of traffic emissions;
- the behaviour of material released into street-canyons;
- the chemical reactions occurring between nitrogen oxides, ozone and Volatile Organic Compounds (VOCs);
- the pollution entering a study area from beyond its boundaries;
- the effects of complex terrain on the dispersion of pollutants; and
- the effects of a building on the dispersion of pollutants emitted nearby.

Further details of these features are provided below.

Studies of extensive urban areas are necessarily complex, requiring the manipulation of large amounts of data. To allow users to cope effectively with this requirement, ADMS-Urban runs in Windows 10, Windows 8, Windows 7 and Windows Vista environments. The manipulation of data is further facilitated by the possible integration of ADMS-Urban with a Geographical Information System (GIS) (MapInfo, ArcGIS, or the ADMS-Mapper) and the CERC Emissions Inventory Toolkit, EMIT.

### *Dispersion Modelling*

ADMS and ADMS-Urban use boundary layer similarity profiles to parameterise the variation of turbulence with height within the boundary layer, and the use of a skewed-Gaussian distribution to determine the vertical variation of pollutant concentrations in the plume under convective conditions.

The main dispersion modelling features of ADMS-Urban are as follows:

ADMS-Urban is an **advanced dispersion model** in which the boundary layer structure is characterised by the height of the boundary layer and the Monin-Obukhov length, a length scale dependent on the friction velocity and the heat flux at the surface. This method supersedes methods based on Pasquill Stability Categories, as used in, for example, Caline and ISC. Concentrations are calculated hour by hour and are fully dependent on prevailing weather conditions.

For convective conditions, a **non-Gaussian vertical profile of concentration** allows for the skewed nature of turbulence within the atmospheric boundary layer, which can lead to high concentrations near to the source.

A **meteorological pre-processor** calculates boundary layer parameters from a variety of input data, typically including date and time, wind speed and direction, surface temperature and cloud cover. Meteorological data may be raw, hourly averaged or statistically analysed data.

### *Emissions*

Emissions into the atmosphere across an urban area typically come from a wide variety of sources. There are likely to be industrial emissions from chimneys as well as emissions from road traffic and domestic heating systems. To represent the full range of emissions configurations, the explicit source types available within ADMS-Urban are:

**Roads**, for which emissions are specified in terms of vehicle flows and the additional initial dispersion caused by moving vehicles is also taken into account.

**Industrial points**, for which plume rise and stack downwash are included in the modelling.

**Areas**, where a source or sources is best represented as uniformly spread over an area.

**Volumes**, where a source or sources is best represented as uniformly spread throughout a volume.

In addition, sources can also be modelled as a regular grid of emissions. This allows the contributions of large numbers of minor sources to be efficiently included in a study while the majority of the modelling effort is used for the relatively few significant sources.

ADMS-Urban can be used in conjunction with CERC's Emissions Inventory Toolkit, EMIT, which facilitates the management and manipulation of large and complex data sets into usable emissions inventories.

### *Presentation of Results*

The results from the model can be based on a wide range of averaging times, and include rolling averages. Maximum concentration values and percentiles can be calculated where appropriate meteorological input data have been input to the model. This allows ADMS-Urban to be used to calculate concentrations for direct comparison with existing air quality limits, guidelines and objectives, in whatever form they are specified.

ADMS-Urban can be integrated with the ArcGIS or MapInfo to facilitate both the compilation and manipulation of the emissions information required as input to the model and the interpretation and presentation of the air quality results provided.

## ***Complex Effects - Street Canyons***

ADMS-Urban incorporates two methods for representing the effect of street canyons on the dispersion of road traffic emissions: a basic canyon method based on the *Operational Street Pollution Model (OSPM)*<sup>2</sup>, developed by the Danish National Environmental Research Institute (NERI); and an advanced street canyon module, developed by CERC. The basic canyon model was designed for simple symmetric canyons with height similar to width and assumes that road traffic emissions originate throughout the base of the canyon, i.e. that the emissions are spread across both the road and neighbouring pavements.

The advanced canyon model<sup>3</sup> was developed to overcome these limitations and is our model of choice. It represents the effects of channelling flow along and recirculating flow across a street canyon, dispersion out of the canyon through gaps in the walls, over the top of the buildings or out of the end of the canyon. It can take into account canyon asymmetry and restricts the emissions area to the road carriageway.

## ***Complex Effects - Chemistry***

ADMS-Urban includes the *Generic Reaction Set (GRS)*<sup>4</sup> atmospheric chemistry scheme. The original scheme has seven reactions, including those occurring between nitrogen oxides and ozone. The remaining reactions are parameterisations of the large number of reactions involving a wide range of Volatile Organic Compounds (VOCs). In addition, an eighth reaction has been included within ADMS-Urban for the situation when high concentrations of nitric oxide (NO) can convert to nitrogen dioxide (NO<sub>2</sub>) using molecular oxygen.

In addition to the basic GRS scheme, ADMS-Urban also includes a trajectory model<sup>5</sup> for use when modelling large areas. This permits the chemical conversions of the emissions and background concentrations upwind of each location to be properly taken into account.

---

<sup>2</sup> Hertel, O., Berkowicz, R. and Larssen, S., 1990, 'The Operational Street Pollution Model (OSPM).' *18<sup>th</sup> International meeting of NATO/CCMS on Air Pollution Modelling and its Applications*. Vancouver, Canada, pp741-749.

<sup>3</sup> Hood C, Carruthers D, Seaton M, Stocker J and Johnson K, 2014. Urban canopy flow field and advanced street canyon modelling in ADMS-Urban. 16<sup>th</sup> International Conference on Harmonisation within Atmospheric Dispersion Modelling for Regulatory Purposes, Varna, Bulgaria, September 2014.  
[http://www.harmo.org/Conferences/Proceedings/\\_Varna/publishedSections/H16-067-Hood-EA.pdf](http://www.harmo.org/Conferences/Proceedings/_Varna/publishedSections/H16-067-Hood-EA.pdf)

<sup>4</sup> Venkatram, A., Karamchandani, P., Pai, P. and Goldstein, R., 1994, 'The Development and Application of a Simplified Ozone Modelling System.' *Atmospheric Environment*, Vol 28, No 22, pp3665-3678.

<sup>5</sup> Singles, R.J., Sutton, M.A. and Weston, K.J., 1997, 'A multi-layer model to describe the atmospheric transport and deposition of ammonia in Great Britain.' In: *International Conference on Atmospheric Ammonia: Emission, Deposition and Environmental Impacts*. *Atmospheric Environment*, Vol 32, No 3.

### ***Complex Effects - Terrain***

As well as the effect that complex terrain has on wind direction and, consequently, pollution transport, it can also enhance turbulence and therefore increase dispersion. These effects are taken into account in ADMS-Urban using the FLOWSTAR<sup>6</sup> model developed by CERC.

### ***Data Comparisons – Model Validation***

ADMS-Urban is a development of the Atmospheric Dispersion Modelling System (ADMS), which is used throughout the UK by industry and the Environment Agency to model emissions from industrial sources. ADMS has been subject to extensive validation, both of individual components (e.g. point source, street canyon, building effects and meteorological pre-processor) and of its overall performance.

ADMS-Urban has been extensively tested and validated against monitoring data for large urban areas in the UK and overseas, including London, Birmingham, Manchester, Glasgow, Riga, Cape Town, Hong Kong and Beijing, during projects supported by local governments and research organisations. A summary of published model validation studies is available at [www.cerc.co.uk/Validation](http://www.cerc.co.uk/Validation), with other publications available at [www.cerc.co.uk/publications](http://www.cerc.co.uk/publications).

---

<sup>6</sup> Carruthers D.J., Hunt J.C.R. and Weng W-S. 1988. 'A computational model of stratified turbulent airflow over hills – FLOWSTAR I.' Proceedings of Envirosoft. In: *Computer Techniques in Environmental Studies*, P. Zanetti (Ed) pp 481-492. Springer-Verlag.